Università degli Studi di Roma "Sapienza"

Facoltà di Scienze Matematiche Fisiche e Naturali

Corso di laurea in Fisica

Anno Accademico 2010-2011

Tesi di Laurea Specialistica in Fisica

Properties of the Fermion Hard Sphere Fluid

Relatore:
Prof. Omar Benhar Noccioli

Candidato:
Paolo Pisanti

Contents

Introduction

Historically, the most remarkable results of the hard sphere model have been achieved in the field of fluid dynamics. The structure of a simple liquid is in fact largely determined by geometric factors associated with the packing of the molecular hard cores, being therefore mostly affected by the repulsive short-range interaction [1]. The smoothly varying long-range attraction gives rise to a uniform background potential providing the cohesive energy of the liquid, but has little effect on its structure. Hence, it is reasonable to model the short-range forces between particles with the infinitely steep repulsion of the hard sphere potential. The properties of a given liquid can be then related to those of a hard sphere reference system, which are calculable, whereas the attractive part of the potential is treated as a small perturbation.

The representation of a liquid as a system of hard spheres moving in a uniform attractive potential provides the physical basis to the van der Waals equation of state, yielding a quantitative description of the phase diagram of a number of classical systems. In adition, the presence of a strongly repulsive core is a prominent feature of the pair potentials describing the interaction of a variety of quantum systems.

Using properly adjusted values of the parameters ϵ and σ, the Lennard-Jones potential

$$v_{LJ}(r) = 4\epsilon \left[\left(\frac{\sigma}{r}\right)^{12} - \left(\frac{\sigma}{r}\right)^{6} \right] ,$$

provides an accurate account of the interactions between atoms of both bosonic (^{4}He) and fermionic (^{3}He) liquid helium separated by a distance r.

The solid line of Fig. 1 shows the radial distribution function[1] of a Lennard-Jones fluid obtained from computer simulations at density ρ such that $\rho\sigma^3 = 0.85$ and temperature T such that $T/\epsilon = 0.88$. The open dots represent the results obtained including only the repulsive component of the Lennard-Jones potential, while the dashed line corresponds to the radial distribution function of a hard sphere fluid. It clearly appears that the simple hard core potential provides a remarkably accurate description of the system ground state.

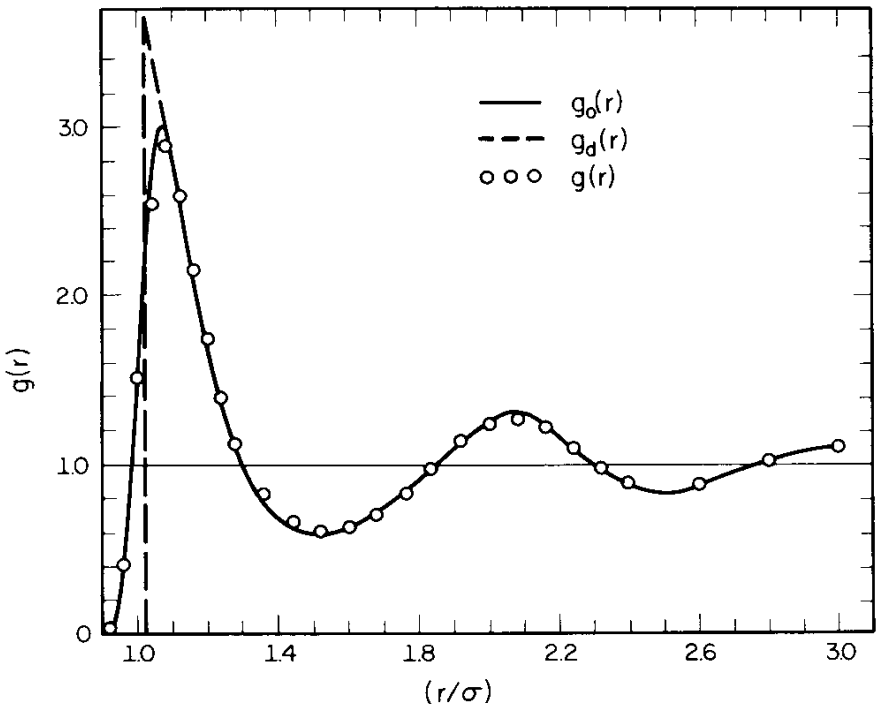

Figure 1: Radial distribution function of a Lennard-Jones fluid at density ρ such that $\rho\sigma^3 = 0.85$ and temperature T such that $T/\epsilon = 088$. Solid line: results of a computer simulation carried out using the full Lennard-Jones potential. Open dots; same as the solid line, but including only the repulsive component of the potential. Dashed line: results of the hard sphere model.

[1]The radial distribution function $g(r)$, to be discussed in Chapter 3, is trivially related to the probability of finding two particles at relative distance r in the system ground state.

The nucleon-nucleon interaction is also known to be strongly repulsive at short distances, as clearly indicated by the saturation of the charge-density distributions measured by elastic electron-nucleus scattering. For this reason the fermion hard sphere fluid, i.e. a system of point-like spin one-half particles interacting through the potential

$$v(r) = \begin{cases} \infty & r < a \\ 0 & r > a \end{cases} ,$$

is a very useful model for investigating concepts and approximations employed to study the properties of nuclear matter.

In this thesis we report the results of calculations of equilibrium and non equilibrium properties of the fermion hard sphere fluid, carried out using the formalism based on correlated basis functions and the cluster expansion technique.

As an introduction, in Chapter 1 we will discuss the approach to the hard sphere problem based on perturbation theory and the low-density expansion, while Chapter 2 is devoted to the description of Correlated Basis Function (CBF) theory and to the derivation of the integral equations for the radial distribution functions of both Bose and Fermi systems.

The results of numerical calculations of the binding energy per particle are presented in Chapter 3, where we also discuss the extension of the CBF approach to the description of transport properties. The calculated values of the shear viscosity coefficient are reported as an example.

Appendices A and B collect some results of scattering theory that are used in the thesis.

Unless otherwise stated, we use a system of units in which $\hbar = h/2\pi = c = K_B = 1$, where h, c and K_B denote Plank's constant, the speed of light and Boltzmann's constant, respectively.

Chapter 1

Perturbative approach

The description of a quantum mechanical system of interacting particles unavoidably requires the use of an approximation scheme, suitable for the determination of the wave-functions and the energy spectrum [2]. In this Chapter we will describe the approach based on many-body perturbation theory and its application to the case in which the interaction potential exhibits a strong repulsive core.

1.1 Mean field approximation

Let us consider a quantum mechanical system consisting of N non-interacting particles obeying Fermi statistics. Their ground state is described by the wave function $|\Phi_0\rangle$, solution of the Schrödinger equation

$$H_0|\Phi_0\rangle = \mathcal{E}_0|\Phi_0\rangle \ , \tag{1.1.1}$$

with

$$H_0 = \sum_{i=1}^{N} \frac{\mathbf{p}_i^2}{2m} \ , \tag{1.1.2}$$

where $\mathbf{p}_i$ and m denote the momentum of the i-th particle and its mass, respectively.

From Eqs. (1.1.1) and (1.1.2) it follows that Φ_0 reduces to the product of wave-functions describing the independent motion a single particle, properly antisymmetrized to account for the effect of Pauli principle.

In the presence of interactions described by a potential $v(r_{ij})$, $r_{ij} = |\mathbf{r}_i - \mathbf{r}_j|$ being the interparticle distance, the hamiltonian becomes

$$H = H_0 + \sum_{j>i=1}^{N} v(r_{ij}) \ , \tag{1.1.3}$$

and the properties of the system are significantly modified. Due to the appearance of interparticle correlations induced by the potential, the exact solution of the Schrödinger equation

$$H|\Psi_0\rangle = E|\Psi_0\rangle \ , \tag{1.1.4}$$

is no longer possible, and one has to resort to approximations.

It is an experimental fact that even in the presence of interactions the independent particle model provides a fairly good description of a number of properties of many-particle systems. The assumption underlying this model is that each particle, say particle i, moves in the mean field resulting from the *average* of its interactions with the remaining $N-1$ particles. The simplest implementation of this scheme amounts to replacing

$$\sum_{j>i=1}^{N} v(r_{ij}) \rightarrow \sum_{i=1}^{N} U(\mathbf{r}_i) \quad , \quad U(\mathbf{r}_i) = \sum_{j\neq i=1}^{N} \langle v(r_{ij}) \rangle \ , \tag{1.1.5}$$

where $\langle \ldots \rangle$ denotes the average over the degrees of freedom of particle j.

Higher order contributions to the mean field can be taken into account within a self-consistent scheme. The Hartree-Fock approximation includes infinite orders of perturbation theory through the substitution of the Green's function of the non-interacting system, G_0 , with the corresponding quantity of the interacting system, G. This procedure is best illustrated by the Feynman diagrams of Fig. 1.1 [2]. It clearly appears that the self-energy insertions are included within a self-consistent scheme, in which the Green's function G both determines and is determined by the proper self energy $\Sigma^\star$ [1]. As a first approxi-

[1] The self-energy insertion is any part of a diagram that is connected to the rest by two particle lines, whereas the proper self-energy insertion is defined as an *irreducible* self-energy insertion (see Fig. 1.1).

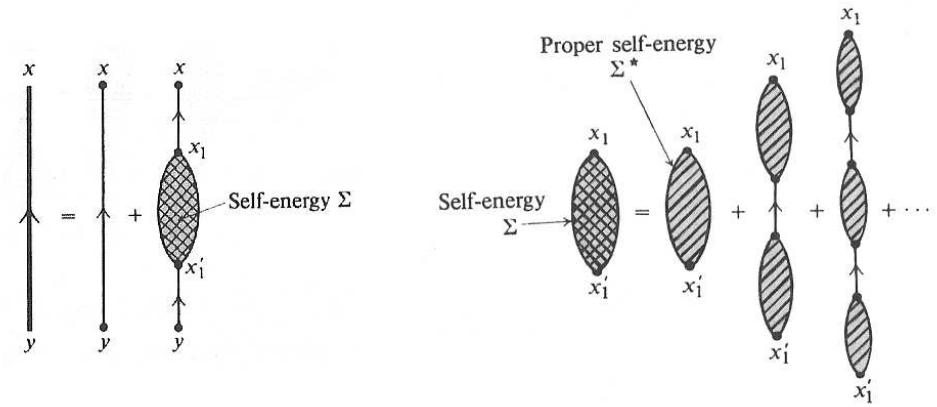

Figure 1.1: Diagrammatic representations of the definition of the Green-function G in terms of G_0 (left panel) and the relation between self-energy (Σ) and proper self-energy ($\Sigma^\star$) (right panel).

mation, one keeps only the first order contribution to the proper self-energy $\Sigma^\star_{(1)}$, which amounts to using the definition of the mean field of Eq.(1.1.5). The corresponding Feynman diagrams are shown in Fig.1.2. In this way, however, the interactions between the

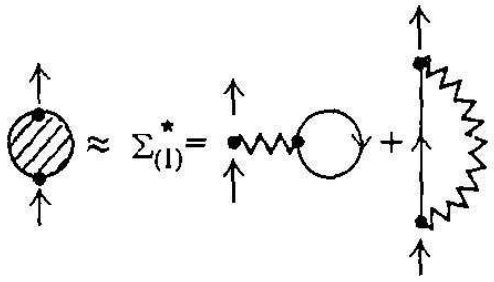

Figure 1.2: Lowest order proper self-energy.

background particles contributing to $\Sigma^\star_{(1)}$ are disregarded. To include their effects we have to replace the thin line (representing the non-interacting Green-function G_0) with the thick line (representing the exact Green-function G), as shown in figure Fig. 1.3.

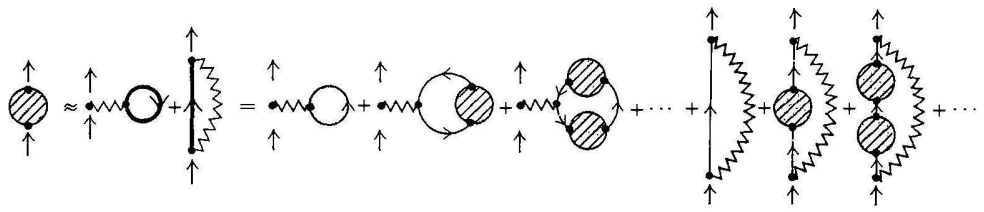

Figure 1.3: Self-consistent proper self-energy in Hartree-Fock approximation.

The mean field approximation has been successfully employed to explain a number of properties of interacting many-particle systems, like, for example, the electronic structure of atoms. However, it is long known to fail when the interaction potential exhibits a strong repulsive core. The source of this problem can be easily understood considering that the matrix element $\langle\phi|v|\phi\rangle$, where ϕ is the wave function describing a pair of non interacting particles, turns out to be large, in fact divergent in the case of hard spheres. As a consequence, the perturbative expansion is, at best, slowly convergent. However, its terms can be rearranged, replacing the potential v with the scattering matrix t, describing scattering processes involving *free* particles. This procedure, which amounts to summing up the so called ladder diagrams to all order, and the resulting low density expansion will be described in Section 1.3. As an introduction, the next Section is devoted to a brief review of scattering theory.

1.2 Review of scattering theory

The results collected in this Section and in Appendices A and B are meant to provide the background material for the discussion of the scattering matrix and the transport properties of the fermion hard sphere fluid.

Let us consider the Schrödinger equation for a generic scattering problem [3],

$$(H_0 + H_1)|\psi\rangle = E|\psi\rangle \ , \tag{1.2.1}$$

where H_0 is the hamiltonian of the unperturbed system, with eigenstate $|\phi\rangle$, H_1 represent a stationary source and $|\psi\rangle$ is the eigenstate of the full hamiltonian. Equation (1.2.1) can be cast in the form

$$|\psi\rangle = |\phi\rangle + \frac{1}{E - H_0} H_1 |\psi\rangle \ , \tag{1.2.2}$$

showing that $|\psi\rangle \to |\phi\rangle$ as $H_1 \to 0$. However, as the operator $1/(E - H_0)$ is singular, one has to provide a prescription to handle its poles. This task is accomplished rewriting Eq.(1.2.2) as

$$|\psi^{\pm}\rangle = |\phi\rangle + \frac{1}{E - H_0 \pm i\epsilon} H_1 |\psi^{\pm}\rangle, \tag{1.2.3}$$

with $\epsilon = 0^+$. Equation (1.2.3) is known as Lipmann-Schwinger (LS) equation.

Multiplying Eq.(1.2.1) by $2m$, where m is the particle mass, and working in coordinate representation we obtain

$$(\nabla^2 + k^2)\psi(\mathbf{r}) = 2m\langle \mathbf{r}|H_1|\psi\rangle, \tag{1.2.4}$$

where $k^2 = 2mE$ and $\psi(\mathbf{r}) = \langle \mathbf{r}|\psi\rangle$. We can transform the above equation into an integral equation using the standard Green's functions technique, based on the relations

$$(\nabla^2 + k^2)G(\mathbf{r}, \mathbf{r}') = \delta(\mathbf{r} - \mathbf{r}') \to G(\mathbf{r}, \mathbf{r}') = \frac{e^{\pm ik|\mathbf{r} - \mathbf{r}'|}}{4\pi|\mathbf{r} - \mathbf{r}'|}. \tag{1.2.5}$$

Making the assumption that the scattering hamiltonian H_1 depends on position only, i.e. that

$$\langle \mathbf{r}|H_1|\mathbf{r}'\rangle = V(\mathbf{r})\delta(\mathbf{r} - \mathbf{r}') \ , \tag{1.2.6}$$

from Eqs.(1.2.3) and (1.2.4) we obtain the integral equation

$$\psi^{\pm}(\mathbf{r}) = \phi(\mathbf{r}) - 2m \int d^3r' \, \frac{e^{\pm ik|\mathbf{r} - \mathbf{r}'|}}{4\pi|\mathbf{r} - \mathbf{r}'|} V(\mathbf{r}')\psi^{\pm}(\mathbf{r}'), \tag{1.2.7}$$

which can be solved using an iteration scheme, leading to a perturbative expansion for $\psi^{\pm}(\mathbf{r})$.

The solution can be simplified making three further assumptions:

- the initial state is a plane-wave of wave vector $\mathbf{k}$, normalized according to $\langle \mathbf{k}'|\mathbf{k}\rangle = \delta(\mathbf{k}-\mathbf{k}')$;
- the scattering potential $V(\mathbf{r})$ is non-vanishing only in a localized region of space centred at the origin, i.e. at $\mathbf{r}=0$;
- we are interested in the solution $\psi^{\pm}(\mathbf{r})$ far away from the scattering region, i.e. in the region where $\mathbf{r} \gg \mathbf{r}'$, implying $|\mathbf{r}-\mathbf{r}'| \simeq r - \hat{\mathbf{r}}\cdot\mathbf{r}'$ and

$$e^{\pm ik|\mathbf{r}-\mathbf{r}'|} \simeq e^{\pm ikr} e^{\mp i\mathbf{k}'\cdot\mathbf{r}'} \ .$$

Under the above conditions, Eq.(1.2.7) reduces to

$$\psi^{\pm}(\mathbf{r}) = \frac{e^{i\mathbf{k}\cdot\mathbf{r}}}{(2\pi)^{3/2}} - \frac{m}{2\pi}\frac{e^{\pm ikr}}{r}\int d^3r' \; e^{\mp i\mathbf{k}'\cdot\mathbf{r}'} V(\mathbf{r}')\psi^{\pm}(\mathbf{r}') \ . \tag{1.2.8}$$

The first term in the right-hand side is the incident plane-wave, while the second represents a spherical wave. The plus and minus signs in $\psi^{\pm}$ correspond to an outgoing or ingoing wave, respectively. Obviously, only the former represents the physical solution.

The scattering wave function can be conveniently rewritten as

$$\psi^{\pm}(\mathbf{r}) = \frac{1}{(2\pi)^{\frac{3}{2}}}\Big[e^{i\mathbf{k}\cdot\mathbf{r}} + \frac{e^{ikr}}{r} f(\mathbf{k},\mathbf{k}')\Big], \tag{1.2.9}$$

where

$$\begin{aligned} f(\mathbf{k},\mathbf{k}') &= -(2\pi)^2 m \int d^3r' \; \frac{e^{-i\mathbf{k}'\cdot\mathbf{r}'}}{(2\pi)^{3/2}} V(\mathbf{r}')\psi^{\pm}(\mathbf{r}') \\ &= -(2\pi)^2 m \langle \mathbf{k}'|H_1|\psi\rangle, \end{aligned} \tag{1.2.10}$$

is the scattering amplitude. It can be easily seen that the differential cross-section of the process in which a particle carrying momentum $\mathbf{k}$ is scattered within a solid angle $d\Omega$

about the direction of the final momentum $\mathbf{k}'$, with $|\mathbf{k}| = |\mathbf{k}'|$, can be expressed in terms of the scattering amplitude according to

$$\frac{d\sigma}{d\Omega} = |f(\mathbf{k}, \mathbf{k}')|^2 \ . \tag{1.2.11}$$

Equation (1.2.9) states that, in general, the total scattering wave function is a superposition of the incident plane wave and a spherical wave propagating from the center of the scattering region. However, if the interaction driving the scattering process is weak, $\psi(\mathbf{r})$ does not differ significantly from the incident wave $\phi(\mathbf{r})$, and one can make the approximation, referred to as Born approximation,

$$\psi(\mathbf{r}) \sim \frac{e^{i\mathbf{k}\cdot\mathbf{r}}}{(2\pi)^{3/2}} \ , \tag{1.2.12}$$

leading to the following form of the scattering amplitude

$$f(\mathbf{k}, \mathbf{k}') = -m(2\pi)^2 \int d^3r' \ e^{i(\mathbf{k}-\mathbf{k}')\cdot\mathbf{r}'} \, V(\mathbf{r}') \ . \tag{1.2.13}$$

The partial wave expansion of the scattering amplitude and the application to a scattering process involving two hard spheres is discussed in Appendices A and B.

1.3 Low density expansion

We will now apply the results discussed in the previous Section to develop an approximation scheme suitable for the description of the hard sphere fluid.

To properly include the effects of the hard core, the first step is the calculation of the scattering matrix in free space. The modifications arising from the presence of the background particles are then included as corrections. It has to be kept in mind that a truly infinite repulsive core causes divergences at all orders in perturbation theory. Hence, one has to consider instead a strong but finite potential V_0, and take the limit $V_0 \to \infty$ at the end of the calculations.

1.3.1 Summation of ladder diagrams

For a finite potential V_0 we can expand the right hand side of equation Eq.(1.2.7), with the result

$$\begin{aligned}\psi^+(\mathbf{r}) = \frac{1}{(2\pi)^{\frac{3}{2}}}\Bigg[e^{i\mathbf{k}\cdot\mathbf{r}} - \int d^3r'\, G(\mathbf{r},\mathbf{r}')v(\mathbf{r}')e^{i\mathbf{k}\cdot\mathbf{r}'} \\ + \int d^3r'\, d^3z'\, G(\mathbf{r},\mathbf{r}')v(\mathbf{r}')G(\mathbf{r},\mathbf{z}')v(\mathbf{z}')e^{i\mathbf{k}\cdot\mathbf{z}'} + \dots\Bigg]\,,\end{aligned} \tag{1.3.1}$$

where $v(\mathbf{r}') \equiv 2mV(\mathbf{r}')$. The above expression can be intuitively interpreted as the unperturbed solution plus corrections involving an increasing number of interaction vertices. We can collect these terms in the perturbation series, represented diagrammatically in Fig. 1.4, to obtain

$$-4\pi f(\mathbf{k},\mathbf{k}') = \int d^3r' e^{-i\mathbf{k}\cdot\mathbf{r}'} V(\mathbf{r}')\psi^+(\mathbf{r}'). \tag{1.3.2}$$

In the case of weak potential the scattering amplitude is well described by the first few terms of the expansion Eq.(1.3.1), or even at the level of the Born approximation discussed in the previous Section. However, the description of scattering from a strongly repulsive potential requires the inclusion of all terms. Similarly, the first-order proper self-energy of Fig.1.2 is not accurate enough for a strong potential and must be corrected

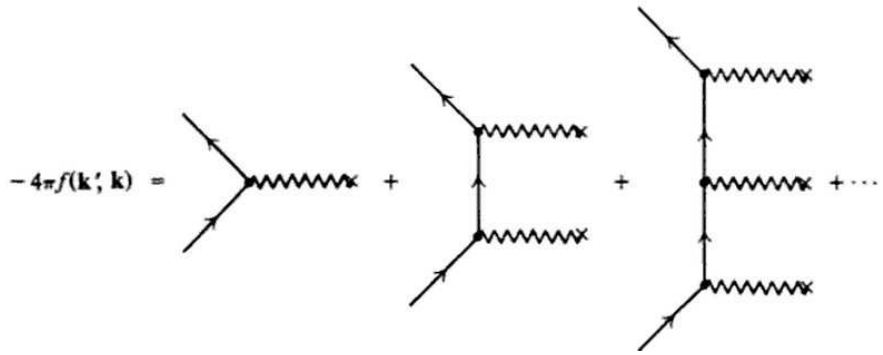

Figure 1.4: Perturbation expansion for two-body scattering amplitude in free space.

including selected higher-order terms. The corresponding diagrams, shown in Fig.1.5, feature repeated interactions, describing the action of the potential on the wave function at all orders. The relevant quantity in this expansion will then be the product $V_0\psi$ or, more generally, the two-body scattering amplitude $f(\mathbf{k}, \mathbf{k}')$, which remains well defined even after taking the $V_0 \to \infty$ limit.

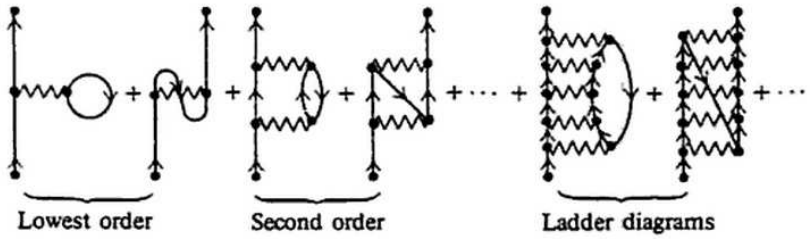

Figure 1.5: Sum of ladder diagrams for the proper self-energy.

1.3.2 Energy per particle

The formalism outlined in the previous Sections can be employed to develop an expansion suitable for describing the properties of a *dilute* interacting Fermi system. Consider, for example, the ground-state energy per particle. It can be expanded in series of powers

of the small adimensional parameter $x = k_F a$, where a is the scattering length associated with the interaction potential (see Appendix A) and the Fermi momentum k_F is related to the particle density $\rho = N/V$ through

$$k_F = \left(\frac{6\pi^2\rho}{\nu}\right)^{1/3} , \tag{1.3.3}$$

ν being the degeneracy of the momentum eigenstates. Note that for hard sphere systems a coincides with the radius of the hard core.

Keeping terms up to third order, we obtain the expression

$$\frac{E}{N} = \frac{k_F^2}{2m}\left[A + B(k_F a) + C(k_F a)^2 + \dots\right] , \tag{1.3.4}$$

which is obviously meaningful either in the small scattering length ($a \to 0$) or in the low-density ($k_F \to 0$) limit.

Equation (1.3.4) is the counterpart of the expansion of the wave function, Eq.(1.3.1). For a fermion hard-sphere fluid the diagrams represented in Fig. 1.5 allow one to determine the coefficients A, B and C appearing in the right hand side.

The physical interpretation of the terms appearing in the right hand side of Eq.(1.3.4) is the following. The first term is the energy of the non-interacting Fermi gas, while the second, linear in the scattering length, corresponds to forward scattering processes and takes into account both direct and exchange contributions. Forward scattering dominates in the low-density limit, as low-density also implies low-energy collisions, with $|\mathbf{k}| = |\mathbf{k}'| \to 0$. In this regime, the scattering amplitude reduces to (see Appendix A)

$$f(\mathbf{k}, \mathbf{k}') \to -a . \tag{1.3.5}$$

It should be noted that the presence of the medium leads to modifications of the scattering length, as the background particles reduce the phase space available to the interacting pair in the intermediate states. For example, the effect of Pauli principle appears when

a particle is excited above the Fermi sea and then de-excited, leading to a correction of order $(k_F a)^2$. This is the origin of the second contribution to the ground state energy. Any other process involves at least three-particles collision, and yields a power of $(k_F a)^3$.

We now want to show how the coefficients of Eq.(1.3.4) can be determined. Consider the simple case of two fermions interacting through a spin-independent non-singular potential.

The lowest-order ground-state energy is obtained from the matrix elements of the proper self-energy

$$\Sigma^\star(\mathbf{k}) = nV(0) - \frac{1}{(2\pi)^3}\int d^3k'\, V(\mathbf{k}-\mathbf{k}')\,\theta(k_F - k')\ , \tag{1.3.6}$$

between plane wave states. Including the energy of the non interacting system we obtain

$$E = \nu\frac{V}{(2\pi)^3}\int d^3k\,\left[\epsilon^0_{\mathbf{k}} + \tfrac{1}{2}\Sigma^\star(\mathbf{k})\right]\theta(k_F - k), \tag{1.3.7}$$

and using the two above equations we can write the lowest-order ground-state energy in the form

$$\frac{E}{V} = \frac{3}{5}\frac{k_F^2}{2m}\frac{N}{V} + \int_0^{k_F}\frac{d^3k}{(2\pi)^3}\int_0^{k_F}\frac{d^3k'}{(2\pi)^3}\left[2V(0) - V(\mathbf{k}-\mathbf{k}')\right]. \tag{1.3.8}$$

From the definition Eq.(1.3.2), in the low-energy limit of Eq.(1.3.5), we find

$$V(0) \equiv \int d^3x V(x) = -\frac{4\pi}{m} f_{\rm B}(\mathbf{k},\mathbf{k}') \to \frac{4\pi}{m}a_{\rm B}, \tag{1.3.9}$$

where the subscript B refers to the Born approximation discussed in the previous Section, implying $\psi^+(\mathbf{x}) \sim e^{i\mathbf{k}\cdot\mathbf{x}}$. Obviously, one can improve up the above approximation replacing

$$a_{\rm B} \to a \tag{1.3.10}$$

where a is the true scattering length for two-particle scattering in free space.

In the low-density limit we can also use the approximation

$$V(\mathbf{k}-\mathbf{k}') \sim V(0)$$

in the integral of Eq.(1.3.8), to obtain

$$\frac{E}{N} = \frac{k_F^2}{2m}\Big[\frac{3}{5} + \frac{2}{3\pi}(k_F a) + \dots\Big]. \tag{1.3.11}$$

Higher-order terms can be analyzed in a similar fashion. The final expression for a hard sphere systems of degeneracy $\nu = 2$ is [2]

$$\frac{E}{N} = \frac{k_F^2}{2m}\Big[\frac{3}{5} + \frac{2}{3\pi}(k_F a) + \frac{4}{35\pi^2}(11 - 2\ln 2)(k_F a)^2 + 0.23(k_F a)^3 + \dots\Big]\,. \tag{1.3.12}$$

As pointed out above, the first, second and third term are, respectively, the kinetic energy of a free Fermi gas, the correction due to the forward scattering from the particles in the medium and the one due to the Pauli blocking of the intermediate states. The final term, of order $(k_F a)^3$, is related to three-particle correlations.

Chapter 2

Correlated basis function theory

In the previous Chapter we have discussed the approach to the quantum mechanical many-body problem based on perturbation theory in the basis of eigenstates of the hamiltonian of the non interacting system. Within this scheme, the problem of computing the matrix elements of a potential featuring a hard core is circumvented replacing the bare potential with the well behaved scattering matrix, obtained from the solution of the Lipmann-Schwinger equation.

Correlated Basis Function (CBF) perturbation theory [4] provides an alternative approach to handle the hard core problem, in which the basis functions are modified in such a way as to incorporate the main effects of the strongly repulsive interaction at short range. As a results, the matrix elements of the *bare* potential in the correlated basis are small and perturbative expansions are rapidly convergent.

The main problem associated with the CBF approach lies in the calculation of matrix elements using correlated states, which involves $3N$ dimensional integrations. This difficulty is overcome exploiting the cluster expansion formalism, originally developed to obtain the partition function of classical liquids [1, 5]. In this Chapter we will discuss the application of the cluster expansion technique to the calculation of the radial distribution function of quantum liquids obeying both Bose and Fermi statistics.

2.1 Correlated basis functions

The set of correlated wave functions is obtained from the wave functions of the non interacting system through the transformation

$$\Psi_n(1,\ldots,N) = F(1,\ldots,N)\Phi_n(1,\ldots,N) \ , \tag{2.1.1}$$

where F describes the correlation structure, while Φ_n is an independent particle wave function accounting for the symmetry properties of the system. For example, in the case of the ground state of a system of fermions, Φ_0 is a determinant of single particle wave functions associated with the states belonging to the Fermi sea.

The correlation factor $F(1,\ldots,N)$ is symmetric with respect to permutations of its arguments and translationally invariant. Hence it only depends on relative distances between particles. In this work, we will use the simple *ansatz* originally proposed by Jastrow [6]

$$F = \prod_{1\le i<j}^{N} f_{ij}, \tag{2.1.2}$$

$f_{ij} = f(r_{ij})$ being the two-particle correlation functions. The shape of f_{ij} is determined through minimization of the expectation value of the hamiltonian in the correlated ground state

$$\langle H\rangle = \frac{\langle\Phi_0|FHF|\Phi_0\rangle}{\langle\Phi_0|FF|\Phi_0\rangle} \ , \tag{2.1.3}$$

to be discussed in the next Chapter, and reflects the behavior of the interaction potential. Ritz's variational principle states that $\langle H\rangle$ provides an upper bound to the ground state energy. As an example, Fig. 2.1 shows the correlation function for a fluid of fermion hard spheres of radius $a = 1$ fm and degeneracy $\nu = 2$, at density $\rho = 0.0042$ fm^{-3}. It clearly appears that f_{ij} is short ranged and vanishes in the hard core region.

The evaluation of matrix elements of any many-body operator using correlated states involves $3N$-dimensional integration. This problem, which becomes intractable for large

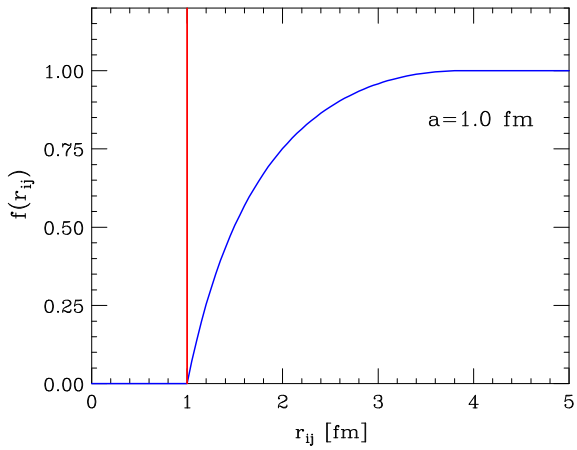

Figure 2.1: Two-particle correlation function for fluid of fermion hard sphere of radius $a = 1$ fm and degeneracy $\nu = 2$ at density $\rho = 0.0042$ fm^{-3}.

N, is circumvented expanding the matrix element in a series, the terms of which represent the contributions of subsystems (clusters) involving an increasing number of particles. Therefore, the evaluation of the cluster contributions requires integrations over the coordinates of a the subset consisting of n particles, with $n = 1, \ldots, N$.

As correlations are short-ranged, at not too high density the cluster expansion is expected to be rapidly convergent. In addition, selected classes of cluster contributions can be summed up at all orders solving the Hyper-Netted-Chain (HNC) [1, 5] of Fermi-Hyper-Netted-Chain (FHNC) [7, 8] integral equations, to be discussed in Sections 2.4 and 2.5, respectively.

Note that the correlation operator defined by Eq.(2.1.2) exhibits the cluster decomposition property, i.e. reduces to the product of two factors according to

$$F(1, \ldots, N) \to F_p(i_1, ..., i_p) F_{N-p}(i_{p+1}, ..., i_N) \ , \tag{2.1.4}$$

when particles $i_1, \ldots, i_p$, are moved far away from the remaining $N - p.$, The above equation expresses the basic tenet underlying the cluster expansion scheme.

Besides *dynamical* correlations, in fermion systems the antisymmetrization of the states

required by Pauli exclusion principle leads to the appearance of additional correlations, of *statistical* origin.

To see this, consider the ground state wave function of a many-body system at uniform density ρ. It can be written in the form

$$\Phi_0 = \det |\varphi_{\alpha_i}(i)| \quad , \qquad \varphi_{\alpha_i}(i) = \frac{1}{\sqrt{V}} \mathrm{e}^{i\mathbf{k}_i\cdot\mathbf{r}_i}\eta_i \ , \tag{2.1.5}$$

where $|\mathbf{k}_i| \leq k_F$, k_F being the Fermi momentum, and ν is the degeneracy of the momentum eigenstates ($\nu = 2$ for spin degeneracy, $\nu = 4$ for spin-isospin degeneracy). The plane waves are normalized in a cubic box of volume $V = L^3$ and satisfy periodic boundary conditions[1]. Finally, η_i describes the discrete (spin or spin-isospin) degrees of freedom. In the case of Bose statistics, Eq.(2.1.5) reduces to

$$\Phi_0 = \sqrt{\frac{N!}{V^N}} \ . \tag{2.1.6}$$

For future use, we give here the expression of the density-matrix associated with the many-body wave function Φ_0

$$\ell(k_F r_{ij}) = \sum_\alpha \varphi^\dagger_\alpha(i)\varphi_\alpha(j) = \frac{\nu}{V}\sum_{|\mathbf{k}|<k_F} e^{i\mathbf{k}\cdot\mathbf{r}_{ij}}, \tag{2.1.7}$$

yielding

$$\ell(x) = \frac{3}{x^3}\big(\sin x - x\cos x\big) \ , \tag{2.1.8}$$

The function $\ell(x)$, whose shape is illustrated in Fig. 2.2, is generally referred to as Slater function. It clearly appears that its value at $x \to 0$ is driven by the degeneracy ν, while its range is determined by the Fermi momentum, i.e. by the density.

[1]The thermodynamic limit corresponds to $N, V \to \infty$, with $\rho = N/V$ finite

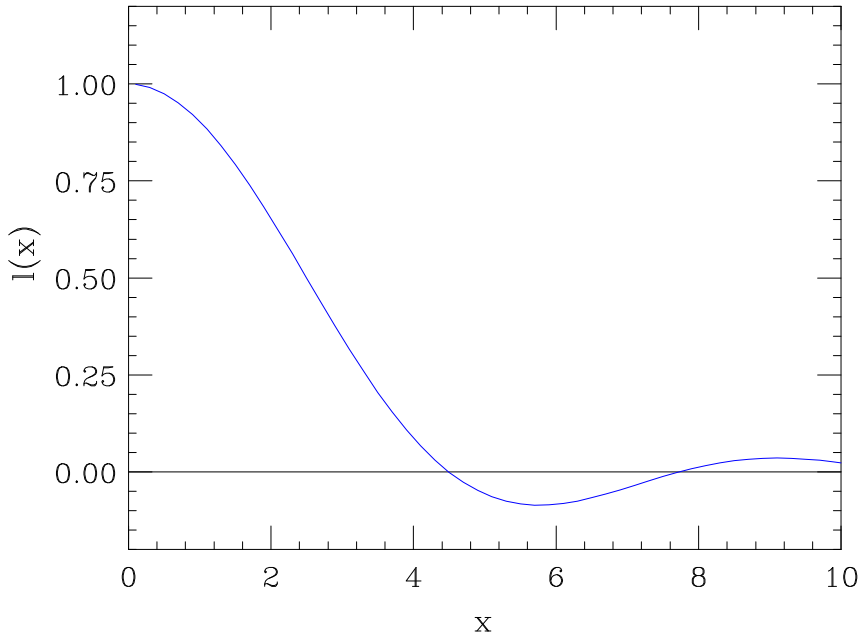

Figure 2.2: Behavior of the Slater function defined in Eq.(2.1.8).

2.2 n-particle distribution functions

The probability of finding n particles at positions $\mathbf{r}_1, \ldots, \mathbf{r}_n$ in the ground state of a quantum fluid is given by [4]

$$p^{(n)}(\mathbf{r}_1, \ldots, \mathbf{r}_n) = \frac{N!}{(N-n)!} \frac{\int dx_{n+1} \ldots dx_N |\Psi_0(1, \ldots, N)|^2}{\int dx_1 \ldots dx_N |\Psi_0(1, \ldots, N)|^2} \ , \tag{2.2.1}$$

where dx_i denotes both integration over $\mathbf{r}_i$ and summation over the discrete degrees of freedom (spin, or spin-isospin) specifying the state of the i-th particle. Note that the above equation implies the normalization

$$\int dx_1 \ldots dx_n \ p^{(n)}(\mathbf{r}_1, \ldots, \mathbf{r}_n) = \frac{N!}{(N-n)!} \ . \tag{2.2.2}$$

In uniform systems the n-particle distribution function defined by Eq.(2.2.1) takes the simple form

$$p^{(n)}(\mathbf{r}_1, \ldots, \mathbf{r}_n) = \rho^n g_n(\mathbf{r}_1, \ldots, \mathbf{r}_n) \ , \tag{2.2.3}$$

showing that the function g_n accounts for the modifications of the distribution function with respect to the one predicted by the independent particle model. Obviously, $p^{(1)}(\mathbf{r}_1) = \rho$, while for $n = 2$ we find

$$p^{(2)}(\mathbf{r}_1, \mathbf{r}_2) = \rho^2 g_2(\mathbf{r}_1, \mathbf{r}_2) = \rho^2 g(r_{12}) \ , \tag{2.2.4}$$

where the so called radial distribution function $g(r)$, exhibiting the asymptotic behavior

$$\lim_{r\to\infty} g(r) = 1 + \mathcal{O}\left(\frac{1}{N}\right) \ , \tag{2.2.5}$$

is related to the measurable liquid structure function, $S(k)$, through

$$S(k) = 1 + \rho \int d^3r \big[g(r) - 1\big] \mathrm{e}^{i\mathbf{k}\cdot\mathbf{r}}\, d^3r \ . \tag{2.2.6}$$

The expectation value of the hamiltonian in the correlated ground state can be cast in the form

$$\langle H \rangle = \langle T \rangle + \langle V \rangle \ , \tag{2.2.7}$$

where $\langle T \rangle$ is the kinetic energy contribution, while $\langle V \rangle$ is the interaction energy, that can be written in terms of the radial distribution function g according to

$$\langle V \rangle = \frac{\rho}{2} \int d^3r\, v(r) g(r) \ . \tag{2.2.8}$$

The simplicity of the above equation is deceptive, as all the difficulties associated with the many-body integrations are hidden in the definition of the radial distribution function. In the following Section we will discuss the approximation scheme employed to obtain $g(r)$.

2.3 Diagrammatic cluster expansion

As shown in Fig. 2.1, the functions describing dynamical correlations in the hard sphere fluid satisfy the conditions

$$f(r < a) = 0 \quad , \quad \lim_{r\to\infty} f(r) = 1 \ , \tag{2.3.1}$$

a being the hard core radius. More generally, in the case of a soft repulsive core, the short range behavior of the correlation functions is such that

$$\lim_{r\to 0} f(r) = 0 \ . \tag{2.3.2}$$

If the interaction is short ranged, so is the correlation function f, and the function

$$h(r) = f^2(r) - 1 \tag{2.3.3}$$

is different from zero only in a small region of space. Hence, its volume integral can be used as an expansion parameter. The starting point is the expansion of the squared N-particle correlation factor of Eq.(2.1.2) in powers of h, according to

$$F^2 = \prod_{j<i} f^2(r_{ij}) = \prod_{j<i} [1 + h(r_{ij})] = 1 + \sum_{j<i} h(r_{ij}) + \sum_{j<i<\ldots} h(r_{ij})h(r_{k\ell}) + \ldots . \tag{2.3.4}$$

We can group together the terms involving p particles to obtain symmetric p-body operators h_p

$$\begin{aligned} F^2 &= 1 + \sum_{i<j} h_2(\mathbf{r}_i, \mathbf{r}_j) + \sum_{i<j<k} h_3(\mathbf{r}_i, \mathbf{r}_j, \mathbf{r}_k) + \ldots \\ &= 1 + \sum_{p=2}^{A} \left[\sum_{i_1<\ldots<i_p} h_p(\mathbf{r}_{i_1} \ldots \mathbf{r}_{i_p}) \right] , \end{aligned} \tag{2.3.5}$$

where, for example,

$$h_2(\mathbf{r}_i, \mathbf{r}_j) = h(r_{ij}) \tag{2.3.6}$$

and

$$h_3(\mathbf{r}_i, \mathbf{r}_j, \mathbf{r}_k) = h(r_{ij})h(r_{ik}) + h(r_{ik})h(r_{jk}) + h(r_{ij})h(r_{jk}) + h(r_{ij})h(r_{jk})h(r_{ik}). \tag{2.3.7}$$

The contributions to the operators h_p can be represented by diagrams in which each factor $h(r_{ij})$ corresponds to a dashed line connecting points i and j. Figure 2.3 shows the diagrams representing the two- and three-body operators. The full set of diagrammatic rules will be given below.

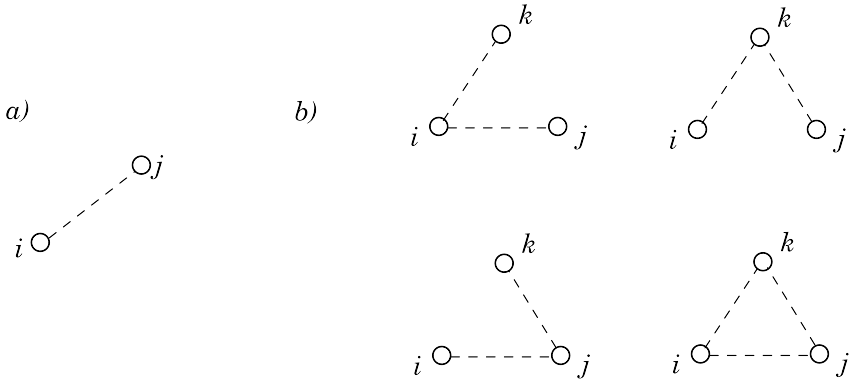

Figure 2.3: Diagrams representing the two- (a) and three-particle (b) operators h_2 and h_3, defined by Eqs.(2.3.6) and (2.3.7), respectively.

In order to use the expansion in p-particle operators for the calculation of the radial distribution function $g(r_{12})$ it is convenient to rearrange the cluster terms in such a way that each of them involve particles 1 and 2 plus an increasing number, $p-2$, of the remaining particles. Applying this procedure we obtain

$$F^2 = X_2(1,2) + \sum_{i_3=3}^{N} X_3(1,2,i_3) + \sum_{i_4>i_3=3}^{N} X_4(1,2,i_3,i_4) + \dots \ . \tag{2.3.8}$$

We can now substitute the above result in the definition of $g(r_{12})$. The symmetry of $|\Phi_0(1,\dots,N)|^2$ with respect to interchange of the particle labels allows us to collect together all the X_p that differ only in the labels of their arguments. As a result, we obtain

$$\begin{aligned} g(r_{12}) &= \frac{N(N-1)}{\rho^2 \mathcal{N}} \int dx_3 \dots dx_N \Delta(1,\dots,N) \\ &\times \sum_{p=2}^{N} \frac{(N-2)!}{(N-p)!(p-2)!} X_p(1,2,\dots,p) \end{aligned} \tag{2.3.9}$$

where

$$\Delta(1,\ldots,N) = |\Phi_0(1,\ldots,N|^2 \ , \tag{2.3.10}$$

and

$$\mathcal{N} = \int dx_1 \ldots dx_N \Delta(1,\ldots,N) F^2(1,\ldots,N) \ . \tag{2.3.11}$$

The function Δ can be readily integrated over the degrees of freedom of particles $p+1,\ldots,N$. From the definition

$$\Delta_p(1,\ldots,p) = \frac{1}{(N-p)!} \int dx_{p+1} \ldots dx_N \Delta(1,\ldots,N) \tag{2.3.12}$$

it follows that the functions Δ_p satisfy the relations

$$\int dx_{p+1} \Delta_{p+1} = (N-p)\Delta_p \ , \tag{2.3.13a}$$

$$\Delta_p \equiv 0 \quad \text{for} \quad p > N \ . \tag{2.3.13b}$$

Note that Eq.(2.3.12) implies that the radial distribution function of the non interacting Fermi gas can be written in the form

$$g_{FG}(r_{12}) = \frac{N(N-1)}{\rho^2} \frac{\int dx_3 \ldots dx_N \Delta(1,\ldots,N)}{\int dx_1 \ldots dx_N \Delta(1,\ldots,N)} = \frac{1}{\rho^2} \Delta_2(r_{12}) \ . \tag{2.3.14}$$

The explicit calculation using Eq.(2.1.5) yields the result

$$g_{FG}(r_{12}) = \frac{1}{\rho^2} \sum_{i,j} \varphi_i^\dagger(\mathbf{r}_1) \varphi_j^\dagger(\mathbf{r}_2) \big[\varphi_i(\mathbf{r}_1)\varphi_j(\mathbf{r}_2) - \varphi_j(\mathbf{r}_1)\varphi_i(\mathbf{r}_2)\big] = 1 - \frac{1}{\nu} \ell^2(k_F r_{12}), \tag{2.3.15}$$

showing that statistical correlations, responsible for the deviation of g_{FG} from unity, are described by the Slater function. The radial dependence of $g_{FG}(r)$ at $k_F = 0.5$ fm^{-1} and degeneracy $\nu = 2$ and 4 is shown in Fig. 2.4.

The cluster contributions appearing in the right hand side of Eq.(2.3.9) can be represented by diagrams, that can be classified according to their topological structures.

A diagram associated with a n-particle cluster consists of n points connected by lines representing dynamical and statistical correlations.

Classification of points:

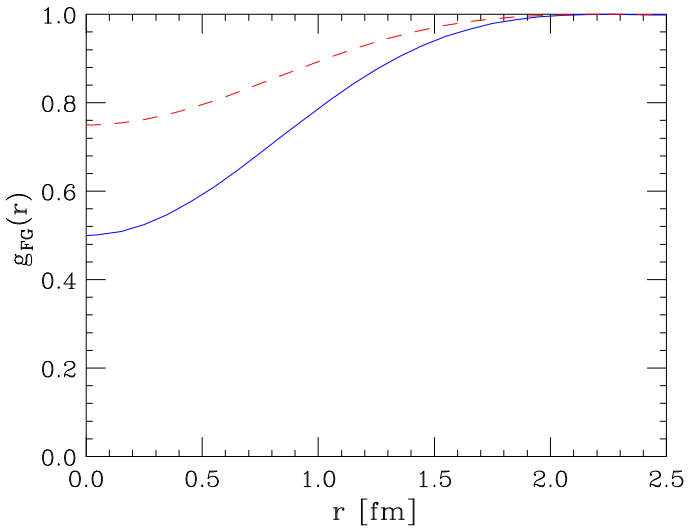

Figure 2.4: Fermi-gas radial distribution function $g_{FG}(r_{12})$, defined by Eq.(2.3.15), at Fermi momentum $k_F = 0.5\,\mathrm{fm}^{-1}$ and degeneracy $\nu = 2$ (solid line) and 4 (dashed line).

- *External points* (*open circles*): represent particles whose degrees of freedom are not integrated over (x_1 and x_2 in the case of the radial distribution function);

- *Internal points* (*solid dots*): represent particles whose degrees of freedom an integration variables. Each internal point contributes a multiplicative factor ρ .

Classification of lines:

- *Dynamical correlation line* (*dashed line*): a line connecting any two points i and j, representing a factor $h(r_{ij})$ in the integrand of the cluster contribution;

- *Statistical correlation line, or exchange line* (*oriented solid lines*): a line connecting any two points i and j, representing a factor $-\ell(k_F r_{ij})/\nu$ in the integrand of the cluster contribution. Obviously, statistical lines are absent in the diagrammatic representation of the radial distribution functions of Bose systems.

Diagrammatic rules:

(i) Every internal point is the extremity of at least one dynamical correlation line:

(ii) No dynamical correlation lines connect pairs of external points;

(iii) Statistical lines form closed non-overlapping loops. A factor $-\nu$ is associated to every loop of statistical lines.

The correlation lines and the corresponding factors are depicted in Fig.(2.5).

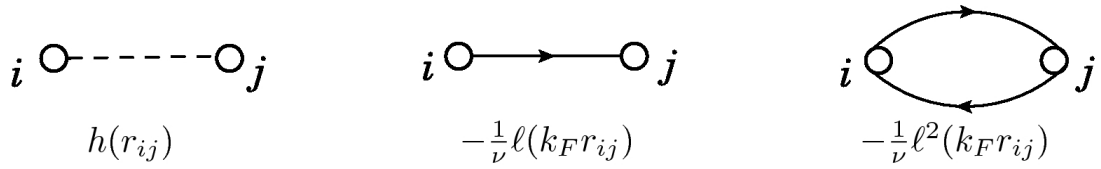

$h(r_{ij})$ $\quad -\frac{1}{\nu}\ell(k_F r_{ij})$ $\quad -\frac{1}{\nu}\ell^2(k_F r_{ij})$

Figure 2.5: Diagrammatic representation of dynamical and statistical statistical correlations lines and the loop of statistical correlation lines involving two particles.

In order to classify the diagrams contributing to the radial distribution function, we first exploit Eq.(2.3.13b) to extend to infinity the upper limit of the summation appearing in Eq.(2.3.9), with the result

$$g(r_{12}) = \frac{N!}{\mathcal{N}\rho^2} \sum_{p=2}^{\infty} \frac{1}{(p-2)!} \int dx_3 \dots dx_p \Delta_p(1,\dots,p) X_p(1,\dots,p)\,. \tag{2.3.16}$$

The product $\Delta_p X_p$ can be factorized in two parts. The diagrams associated with the first one, $C_n(1,2,i_3,\dots,i_n)$, contain the external points, 1 and 2, plus a set of internal points, connected to the external points by at least one continuous path of dynamical or statistical correlation lines. The diagrams associated with the second factor, $D_{p-n}(i_{n+1},\dots,i_p)$, contain p–n internal points, disconnected from $1,2$ (and therefore from the points of C_n).

Carrying out independently the integration of these two terms and relabeling the

points we find

$$g(r_{12}) = \frac{1}{\mathcal{N}\rho^2}\Big[\sum_{n=2}^{\infty}\int dx_3\ldots dx_n\frac{C_n(1,2\ldots n)}{(n-2)!}\Big]\Big[\sum_{m=0}^{\infty}\int dx_1\ldots dx_m\frac{D_m(1,2\ldots m)}{m!}\Big]\ . \tag{2.3.17}$$

It can be easily shown that the second summation involved in the above equation coincides with the cluster expansion of the normalization integral $\mathcal{N}$. Hence, all the disconnected diagrams appearing in the cluster expansion of the radial distribution function cancel exactly.

The cancellation of the disconnected parts is a very general property of many diagrammatic expansions, which allows us to write

$$g(r_{12}) = \sum_{p=2}^{\infty}\Gamma_p(1,2), \tag{2.3.18}$$

where $\Gamma_p(1,2)$ is the sum of all topologically distinct *connected* diagrams with $1,2$ as external points and $p-2$ points connected to one another in all possible ways.

There is another cancellation leading to a further simplification of the diagrammatic scheme. The connected diagrams can be classified in two classes: the first one contains *reducible* diagrams, i.e. diagrams that can be divided in two or more disconnected parts by cutting the diagram at a point of reducibility P. The parts which do not contain the external points are called *subdiagrams* and denoted by γ_i, while the remaining part are denoted by Γ. The diagrams belonging to the second class are called *irreducible*. Thanks to translation invariance, implying that the correlation functions only depend on relative distances between particles, the reducible diagrams can be written as a product of independent factors.

The authors of Ref.[8] have shown that cluster terms associated with reducible diagrams cancel. In the case of Fermi systems this result holds true for any N, while in Bose systems the cancellation only occurs in the thermodynamic limit. It follows that the

cluster expansion of the radial distribution function is irreducible and Eq.(2.3.18) becomes

$$g(r_{12}) = \sum_{p=2}^{\infty} \Gamma_p^{\mathrm{irr}}(1,2). \tag{2.3.19}$$

Few examples of connected, disconnected and reducible diagrams are shown in Fig. 2.6.

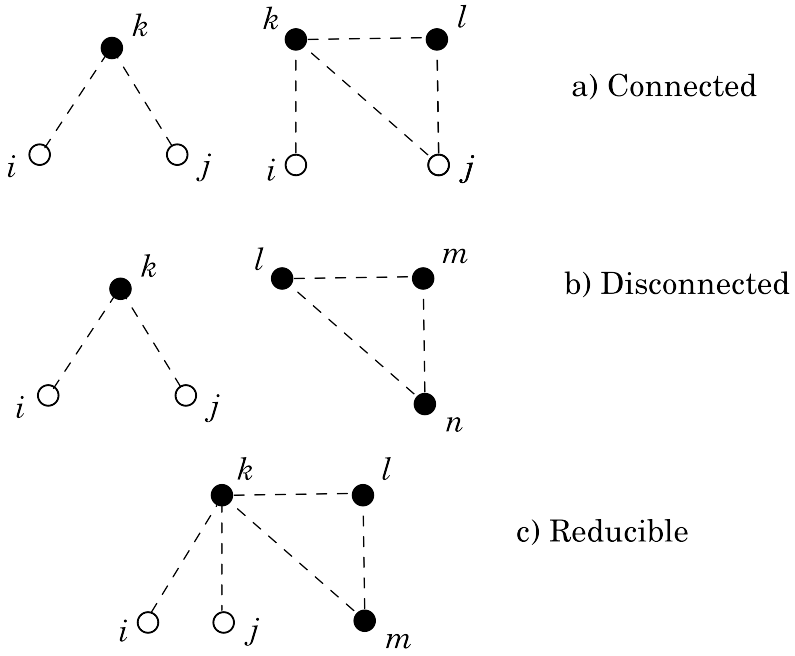

Figure 2.6: Examples of connected, disconnected and reducible diagrams

As a final remark, we note that the cluster contributions appearing in the right hand side of the above equation can be written in such a way that a term $f^2(r_{12})$ appear as a multiplicative factor. In the case of Bose statistic the resulting expansion can be cast in the form

$$g(r_{12}) = f^2(r_{12}) \left[1 + \sum_{p=1}^{\infty} \rho^p g_p(r_{12}) \right] , \tag{2.3.20}$$

where g_p includes the contributions of diagrams involving p internal points. For example, the forst order term reads

$$g_1(r_{12}) = \int d^3 r_3 h(r_{13}) h(r_{32}) \ . \tag{2.3.21}$$

The diagrams representing the first and second order terms in the right hand side of Eq.(2.3.20) are shown in Fig. 2.7. The corresponding expression for the case of Fermi systems will be given in Section 2.5.

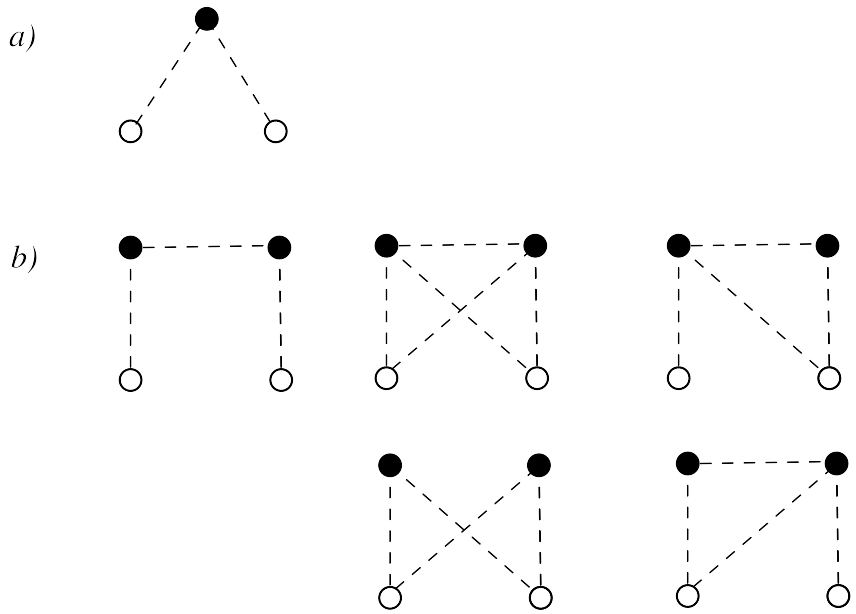

Figure 2.7: Diagrammatic representation of the first (a) and second (b) order contributions to the radial distribution of a Bose fluid, g_1 and g_2 of Eq.(2.3.20).

2.4 Hyper-Netted-Chain (HNC) equation for Bose systems

In the previous Section we have classified the diagrams associated with the terms of the cluster expansion in such a way as to identify those providing vanishing contributions. In this Section we will discuss a further classification, allowing one to sum up selected classes of diagrams to all cluster orders.

To explain the new classification scheme, let us consider first the case of Bose systems

and rewrite Eq.(2.3.20) in the form

$$g(r) = f^2(r_{12})\Big[1 + C(r_{12})\Big] \ , \tag{2.4.1}$$

where the function $C(r_{12})$ consist of the sum of all connected irreducible graphs with $1, 2$ as external points. From these graphs we have to exclude the diagrams with a "short-cut" connection, i.e. a single $h(r_{12})$ bond, between 1 and 2, as such graphs are generated multiplying by $f^2(r_{12}) = 1 + h(r_{12})$.

A *i-j subdiagram* is, by definition, any part of a diagram which is only connected to the rest at points i and j.

A diagram is called *composite* (or *parallel*) if composed by two or more subdiagrams forming parallel independent connections between i and j. A diagram that is not composite is called *simple*.

Since any composite diagram contributing to $C(r_{12})$ consists of a number of simple diagrams connected in parallel, we can express $C(r_{12})$ in terms of simple diagrams only. Denoting $S(r_{12})$ the sum of all irreducible, simple 1-2 diagrams without short-cut bonds $h(r_{12})$, we can write

$$C(r_{12}) = e^{S(r_{12})} - 1 \ , \tag{2.4.2}$$

since expanding the exponential one obtains $S(r_{12})$ plus the sum of all composite diagrams[2]. A 1-2 diagram is called *nodal* if there is at least one point (*node*) all path connecting 1 to 2 must pass through. By definition, a composite diagram is non-nodal. On he other hand, a nodal 1-2 diagram is necessary simple. A simple graph contributing to $C(r_{12})$ may be either nodal or non-nodal; if non-nodal, such a graph is called *elementary*. Hence, we can use the decomposition

$$S(r_{12}) = N(r_{12}) + E(r_{12}) \ , \tag{2.4.3}$$

[2]The factor $1/n!$ associated with the n-th term of the expansion is cancelled exactly by the so called "symmetry number" of the corresponding composite diagrams.

where $N(r_{12})$ and $E(r_{12})$ denote the sum of nodal and elementary diagrams, respectively.

Few examples of diagrams belonging to the classes defined above are depicted in Fig. 2.8 .

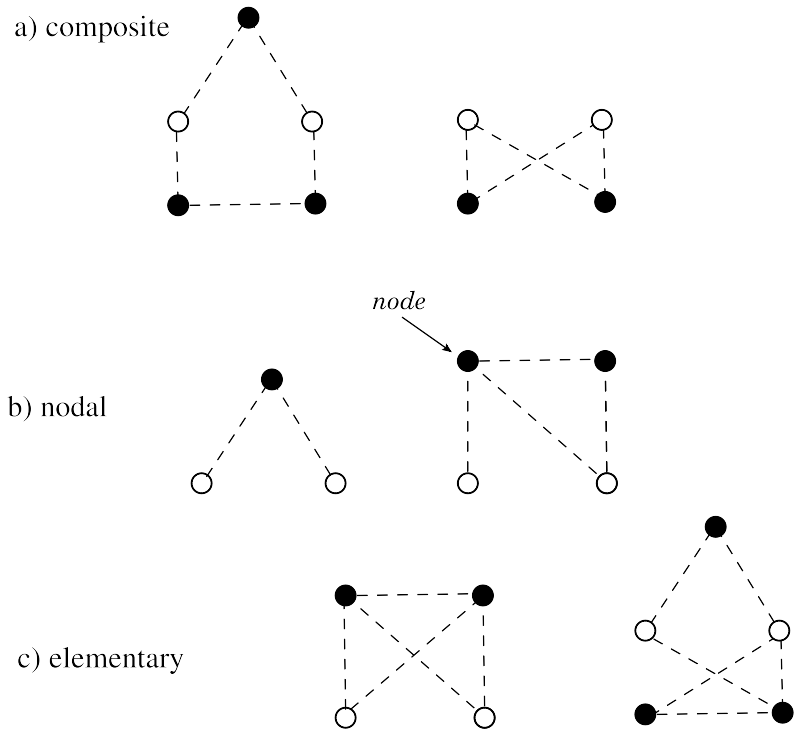

Figure 2.8: Example of generic composite (a) and simple diagrams of nodal (b) and elementary (c) types

From Eq.(2.4.3) it follows that the radial distribution function can be written in the form

$$\begin{aligned} g(r_{12}) &= f^2(r_{12})e^{[N(r_{12})+E(r_{12})]} = f^2(r_{12})\big\{1 + N(r_{12}) + E(r_{12}) + \tfrac{1}{2}[N(r_{12}) + E(r_{12})]^2 + \cdots\big\} \\ &= f^2(r_{12})\big[1 + N(r_{12}) + E(r_{12})\big] + X(r_{12}), \end{aligned} \tag{2.4.4}$$

which defines the function $X(r_{12})$ as the sum of all composite diagrams multiplied by $f^2(r_{12})$.

Figure 2.9 represents the sum of nodal diagrams, N, obtained connecting in series the

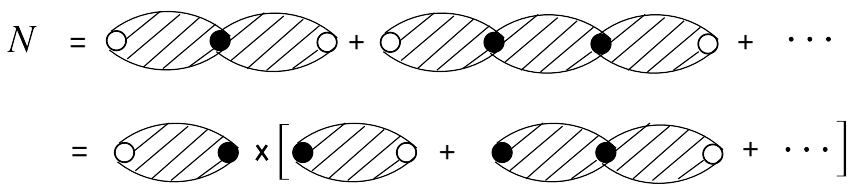

Figure 2.9: Nodal expansion of non-nodal diagrams

X diagrams. It corresponds to the integral equation

$$N(r_{12}) = \rho \int d^3 r_3 \big[X(r_{13}) + N(r_{13})\big] X(r_{32}). \tag{2.4.5}$$

The Hypernetted-chain (HNC) approximation, that can be justified on physics ground at "not too high" densities, amounts to neglecting the elementary diagrams from the expansion of $g(r_{12})$. As a result, one obtains

$$g(r_{12}) = f^2(r_{12}) e^{N(r_{12})} \ , \tag{2.4.6}$$

and

$$X(r_{12}) = f^2(r_{12}) e^{N(r_{12})} - N(r_{12}) - 1 = g(r_{12}) - N(r_{12}) - 1. \tag{2.4.7}$$

Substitution of

$$\frac{g(r_{12})}{f^2(r_{12})} = e^{N(r_{12})} \Rightarrow N(r_{12}) = -\ln f^2(r_{12}) + \ln g(r_{12}) \ , \tag{2.4.8}$$

in Eq.(2.4.7) yields

$$X(r_{12}) = g(r_{12}) - 1 + \ln f^2(r_{12}) - \ln g(r_{12}). \tag{2.4.9}$$

and the integral equation (2.4.5) can be rewritten in the simple form

$$-\ln f^2(r_{12}) + \ln g(r_{12}) = \rho \int d^3 r_3 \big[g(r_{13}) - 1 + \ln f^2(r_{13}) - \ln g(r_{12})\big]\big[g(r_{13}) - 1\big] \ . \tag{2.4.10}$$

The HNC equations for the radial distribution function of a Bose system can be summarized as follows [1, 5]

$$X(r_{12}) = f^2(r_{12})e^{N(r_{12})} - N(r_{12}) - 1 \ , \tag{2.4.11a}$$

$$N(r_{12}) = \rho \int d^3r_3 \big[X(r_{13}) + N(r_{13})\big] X(r_{32}) \ , \tag{2.4.11b}$$

$$g(r_{12}) = X(r_{12}) + N(r_{12}) + 1. \tag{2.4.11c}$$

For any choice of the correlation function $f(r)$, the functions $X(r)$ and $N(r)$ and the radial distribution function $g(r)$ can by obtained from the following procedure

(1) Compute the first approximation to $X(r)$ setting $N(r) = 0$:

$$X^{(0)}(r) = f^2(r) \ ; \tag{2.4.12}$$

(2) Obtain a first approximation to $N(r)$ solving the integral equation (2.4.5), either through matrix inversion or in Fourier space, using

$$N^{(0)}(k) = \frac{\rho X^{(0)}(k)}{1 - \rho X^{(0)}(k)} \ ; \tag{2.4.13}$$

(3) Obtain the first order $X(r)$ from

$$X^{(1)}(r) = f^2(r)e^{N^{(0)}(r)} - N^{(0)}(r) - 1 \ ; \tag{2.4.14}$$

(4) Go back to step (**2**) and continue until convergence is reached.

2.5 Fermi Hyper-Netted-Chain (FHNC) equations

The generalization of the HNC scheme to the case of Fermi system can be easily understood considering that a Bose system can be seen as the limit of its Fermi counterpart for $\nu \to \infty$, with the density ρ kept fixed (note that $k_F \to 0$ as $\nu \to \infty$, so that $\ell(k_F r) \to 1$).

Implementation of Fermi statistic leads to the appearance of statistical (or exchange) correlation lines, that may be superimposed to dynamical correlation lines. The exchange lines fulfill the topological constraint of forming non-overlapping, closed and oriented loops, each loop contributing a factor $-\nu$. As discussed in the previous Sections, only connected and irreducible diagrams contribute.

From the generalization of Eqs.(2.3.19) and (2.3.20), we can obtain the corresponding expansion of the radial distribution function of a Fermi fluid. For example, the term of order ρ becomes

$$\int d^3r_3\, h(r_{13})h(r_{32}) \Rightarrow \int d^3r_3\, h(r_{13})h(r_{32})\Delta_3, \tag{2.5.1}$$

where

$$\Delta_3 = \int d^3r_4 \ldots d^3r_N |\Phi_0(1,\ldots,N)|^2 = 1 - \frac{1}{\nu}\ell^2(k_F r_{12}) - \frac{1}{\nu}\ell^2(k_F r_{13}) - \frac{1}{\nu}\ell^2(k_F r_{32}) + \frac{1}{\nu^2}\ell(k_F r_{12})\ell(k_F r_{23})\ell(k_F r_{32}) + \frac{1}{\nu^2}\ell(k_F r_{13})\ell(k_F r_{32})\ell(k_F r_{21})\ . \tag{2.5.2}$$

The diagrams representing the terms involving $p = 0$ and 1 internal points are shown in Fig. 2.10.

The presence of statistical correlation lines leads to another classification of the $i-j$ diagrams, based on the types of correlation lines reaching points i and j. Denoting $\Gamma(i,j)$ the generic diagram (of N, X or E type), we label can it as

$\Gamma_{dd}(i,j)$ if both i and j are reached by dynamical correlation lines only;

$\Gamma_{de}(i,j)$ if i is reached by a dynamical correlation line only, while j is reached by two statistical correlation lines.

$\Gamma_{ee}(i,j)$ if both i,j are reached by two statistical lines,

$\Gamma_{cc}(i,j)$ if both i,j are reached by one statistical line.

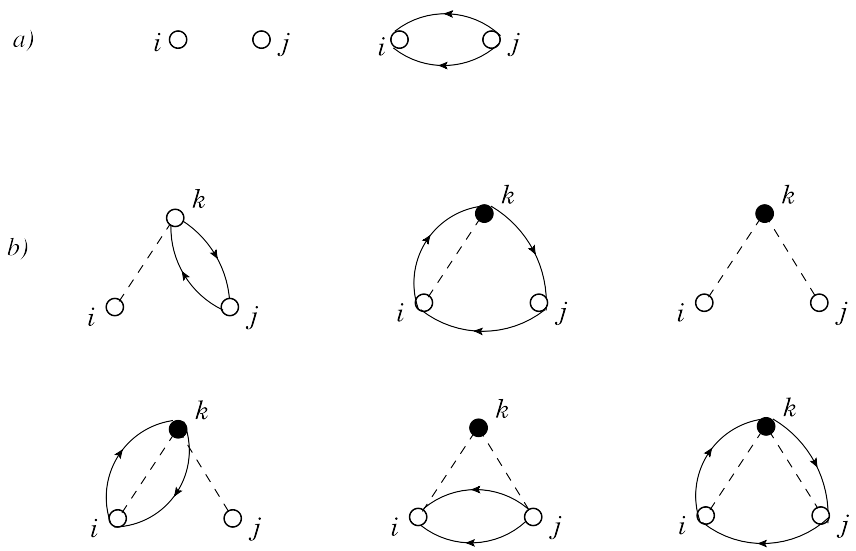

Figure 2.10: Diagrammatic representation of the contributions to the radial distribution function of a Fermi fluid involving $p = 0$ (a) and 1 (b) internal points.

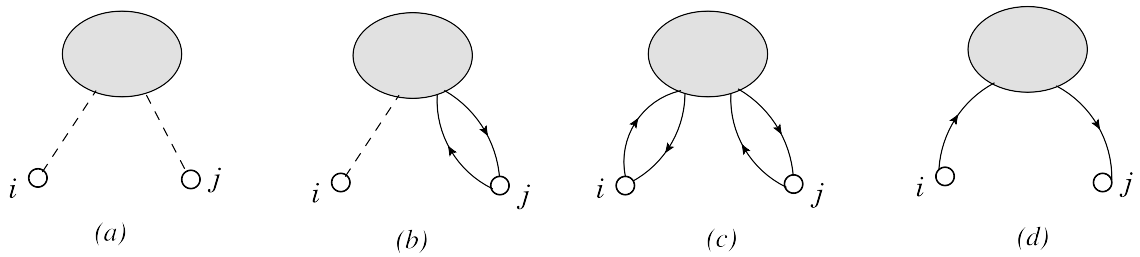

Figure 2.11: Topological structures of Γ_{dd} (a), Γ_{de} (b), Γ_{ee} (c), Γ_{cc} (d) diagrams.

The above classification scheme is illustrated in Fig. 2.11.

The derivation of the integral equations for the nodal functions $N_{xy}(r_{ij})$, analog of

Eq.(2.4.5), is straightforward. The resulting equations read

$$N_{dd}(r_{ij}) = \rho \int d^3r_k \left\{ \left[X_{dd}(r_{ik}) + X_{de}(r_{ik})\right] W_{dd}(r_{kj}) + X_{dd}(r_{ik}) W_{de}(r_{kj}) \right\}, \tag{2.5.3a}$$

$$N_{de}(r_{ij}) = \rho \int d^3r_k \left\{ \left[X_{dd}(r_{ik}) + X_{de}(r_{ik})\right] W_{de}(r_{kj}) + X_{dd}(r_{ik}) W_{ee}(r_{kj}) \right\}, \tag{2.5.3b}$$

$$N_{ee}(r_{ij}) = \rho \int d^3r_k \left\{ \left[X_{de}(r_{ik}) + X_{ee}(r_{ik})\right] W_{de}(r_{kj}) + X_{de}(r_{ik}) W_{ee}(r_{kj}) \right\}, \tag{2.5.3c}$$

$$N_{cc}(r_{ij}) = \rho \int d^3r_k \, X_{cc}(r_{ik}) \left[W_{cc}(r_{kj}) - \frac{1}{\nu}\ell(k_F r_{kj})\right], \tag{2.5.3d}$$

where $W_{xy} \equiv N_{xy} + X_{xy}$.

Defining

$$F(r) = f^2(r)\, e^{N_{dd}(r)}, \tag{2.5.4}$$

we can write the sum of non-nodal diagrams, $X_{xy}(r_{ij})$, given by a set of four equations which are the Fermi analog of Eq.(2.4.5):

$$X_{dd}(r) = F(r) - 1 - N_{dd}(r), \tag{2.5.5a}$$

$$X_{de}(r) = F(r)\, N_{de}(r) - N_{de}(r), \tag{2.5.5b}$$

$$X_{ee}(r) = F(r)\Big\{ N_{ee}(r) + N_{de}^2(r) - \nu[N_{cc}(r) - \frac{1}{\nu}\ell(k_F r)]^2 \Big\} - N_{ee}(r), \tag{2.5.5c}$$

$$X_{cc}(r) = F(r)\left[N_{cc}(r) - \frac{1}{\nu}\ell(k_F r)\right] + \frac{1}{\nu}\ell(k_F r) - N_{cc}(r)\ . \tag{2.5.5d}$$

The radial distribution function can be readily expressed in terms of nodal (N_{xy}) and non nodal (X_{xy}) functions, according to

$$g(r) = 1 + W_{dd}(r) + 2W_{de}(r) + W_{ee}(r). \tag{2.5.6}$$

Equations (2.5.3)-(2.5.6), originally obtained by Fantoni e Rosati [7, 8], are referred to as FHNC equations. Their solutions can be obtained generalizing the iterative procedure described in the previous Section for the case of Bose systems.

Chapter 3

Properties of the hard sphere fluid

The formalism described in the previous Chapter has been employed to obtain a variational estimate of the ground state energy of a system of fermion hard spheres. The expectation value of the hamiltonian, computed solving the FHNC equations, has been minimized with respect to the form of the correlation function. The cluster expansion of the kinetic energy operator, involving some additional difficulties, is discussed in Section 3.1, while the numerical results are presented in Section 3.2.

In Section 3.3 we will discuss the derivation of an effective interaction within the CBF formalism. The effective interaction allows one to develop a consistent treatment of equilibrium and non equilibrium properties of the system. As an example, in Section 3.4 we will show the results of the calculation of the shear viscosity coefficient, obtained using the approach of Landau, Abrikosov and Khalatnikov [10].

3.1 Cluster expansion of the energy expectation value

Following [11], we start defining the generalized normalization integral

$$I(\beta) = \langle \Psi_0 | \exp\left[\beta(H - T_{\rm F})\right] | \Psi_0 \rangle, \tag{3.1.1}$$

where H is the many-body hamiltonian and $T_{\rm F}$ is the ground-state energy of the Fermi gas; it is then possible to rewrite the expectation value of H in the form

$$E = T_{\rm F} + \frac{\partial}{\partial\beta} \ln I(\beta)\Big|_{\beta=0}. \tag{3.1.2}$$

We can also define a set of $N!/(N-n)!n!$ wave-functions describing n-particle subsystems:

$$\Psi_{i_1\ldots i_n} = F_n \Phi_{i_1\ldots i_n}\,, \tag{3.1.3}$$

whit $F_N = F$, $\Phi_{i_1\ldots i_N} = \Phi_0$. These wave-functions allow one to introduce an equivalent set of subnormalization integrals for each subsystem:

$$\begin{aligned} &I_i(\beta) = \langle i|\exp\left[\beta(t(1)-\epsilon_i^F)\right]|i\rangle, \\ &I_{ij}(\beta) = \langle ij|F_2^\dagger(12)\exp\left[\beta(t(1)+t(2)+v(12)-\epsilon_i^F+\epsilon_j^F)\right]F_2(12)|ij\rangle_a\,, \\ &\quad\vdots \\ &I_{1\ldots N}(\beta) = I(\beta), \end{aligned} \tag{3.1.4}$$

where $t(i) = -\nabla_i^2/2m$, ϵ_i^F is the kinetic energy of a particle carrying momentum $\mathbf{k}_i$ and the subscript a on the matrix element indicates that the two-particles states are *antisymmetrized*, i.e.

$$|ij\rangle_a = \frac{1}{\sqrt{2}}(|ij\rangle - |ji\rangle). \tag{3.1.5}$$

We now want to express $\ln I(\beta)$ of Eq.(3.1.2) through the $\ln I_{i_1\ldots i_p}(\beta)$. Noting that I_{ij} reduces to I_iI_j if we neglect $v(12)$ and both dynamical and statistical correlations, we include these effect through a multiplicative factor:

$$I_{ij} = I_iI_jY_{ij}. \tag{3.1.6}$$

The definition of the tensor Y_{ij} can be generalized to any number of indices. From

$$\begin{aligned} &I_i = Y_i, \\ &I_{ij} = Y_iY_jY_{ij}\,, \\ &\quad\vdots \\ &I_{1\ldots N}(\beta) = I = \prod_i Y_i \prod_{j<i} Y_{ij}\ldots Y_{1\ldots N}\,, \end{aligned} \tag{3.1.7}$$

it follows that

$$\ln I(\beta) = \sum_i \ln Y_i + \sum_{j<i} \ln Y_{ij} + \ldots + \ln Y_{1\ldots N}\,. \tag{3.1.8}$$

It can be shown that each term of this sum goes like N in the thermodynamic limit and the n-th term of the series collects all individual contributions to the cluster development of $\ln I(\beta)$ involving, in a connected manner, exactly n Fermi-sea states [11]. It is then correct to interpret the n-th term of Eq.(3.1.8) as the n-body part of $\ln I(\beta)$, or the *n-body cluster*. From the diagrammatic point of view, the n-body cluster is represented by a connected n-point diagram, one point for each particle involved.

The cluster expansion of the energy can be obtained from Eq.(3.1.8):

$$\langle H\rangle = T_{\rm F} + (\Delta E)_1 + (\Delta E)_2 + \ldots + (\Delta E)_N\,, \tag{3.1.9}$$

$$(\Delta E)_n = \sum_{i_1<\ldots<i_n} \frac{\partial}{\partial\beta} \ln Y_{i_1\ldots i_n}(\beta)\Big|_{\beta=0}\,. \tag{3.1.10}$$

Inversion of Eqns.(3.1.7) to express $Y_{ij\ldots}$ in terms of $I_{ij\ldots}$, yields the following expression for the two-body cluster contribution to the energy

$$(\Delta E)_2 = \sum_{i<j} \left[\frac{1}{I_{ij}}\frac{\partial I_{ij}}{\partial\beta} - \Big(\frac{\partial I_i}{\partial\beta} + \frac{\partial I_j}{\partial\beta}\Big)\right]_{\beta=0} = \sum_{i>j} w_{ij}, \tag{3.1.11}$$

where

$$w_{ij} = \langle ij|\tfrac{1}{2}F_2^\dagger(12)\big[t(1)+t(2),F_2(12)\big] + \text{c.c.} + F_2^\dagger(12)v(12)F_2(12)|ij\rangle_a. \tag{3.1.12}$$

Note that we are assuming $F_2^\dagger(12) = F_2(12) = f_{12}$ (see Eq.(2.1.2)). The n-body cluster energy correction of Eq.(3.1.10) can be factorized into *irreducible* contributions given by integrals of simple two-body functions and the Slater factor of Eq.(2.1.7). All reducible or factorizable terms of $(\Delta E)_n$ mutually cancel, as in the expansion of the radial distribution function, discussed in the previous Chapter. More specifically, the two-body cluster term of Eq.(3.1.11) is given by

$$(\Delta E)_2 = \frac{\rho^2}{2}\int w_2(r_{12})\big[1 - \frac{1}{\nu}l^2(k_F r_{12})\big]d^3r_1 d^3r_2, \tag{3.1.13}$$

where

$$w_2(12) = \frac{1}{m}(\nabla f(r_{12}))^2 + f^2(r_{12})v(r_{12}). \tag{3.1.14}$$

3.1.1 Alternative forms for the kinetic energy

The expectation value of kinetic energy in the correlated ground state cannot be computed exactly. The approximations needed to carry out its calculation introduce a degree of ambiguity, arising from the different transformations of the expectation value

$$\begin{aligned} \langle T \rangle &= \frac{1}{\mathcal{N}} \sum_{i=1}^{N} \langle -\frac{\nabla_i^2}{2m} \rangle, \\ \langle -\nabla_i^2 \rangle &= \int \Phi^* \, F \, \nabla_i^2 \, F \, \Phi \;\; d^3r_1 \ldots d^3r_N, \end{aligned} \tag{3.1.15}$$

where $\Phi = \Phi_0$. The straightforward applications of ∇_i^2 to the right gives the so called Pandharipande-Bethe (PB) form [12]

$$\langle -\nabla_i^2 \rangle_{\rm PB} = \int \Phi^* F \big[\nabla_i^2 \Phi + (\nabla_i^2 F)\Phi + 2(\nabla_i F) \cdot (\nabla_i \Phi) \big] d^3r_1 \ldots d^3r_N, \tag{3.1.16}$$

where the contribution of the first term, in which ∇_i^2 operates on the Fermi gas ground state wave function, is

$$T_{\rm F} = \frac{3}{5} \frac{k_F^2}{2m} \; . \tag{3.1.17}$$

As Φ satisfies periodic boundary conditions, surface contributions arising from integration by parts of the third term in the r.h.s. of Eq.(3.1.16) vanish. We can then obtain the Clark-Westhaus (CW) form [13]

$$\langle -\nabla_i^2 \rangle_{\rm CW} = \int \Phi^* \big[F^2 \nabla_i^2 \Phi - (\nabla_i F)^2 \Phi \big] d^3r_1 \ldots d^3r_N \; . \tag{3.1.18}$$

Finally, writing the third term in the r.h.s. of Eq.(3.1.16) as $(\nabla_i F^2) \cdot (\nabla \Phi)$ and integrating by parts we obtain the alternative expression

$$\langle -\nabla_i^2 \rangle = \int \big[-(\nabla_i \Phi^*) F^2 \nabla_i \Phi + \Phi^* F \nabla_i^2 F \, \Phi \, \big],$$

which, using $(\nabla\Phi^*)\cdot(\nabla\Phi) = \big[\nabla(\Phi^*\Phi) - \Phi^*\nabla^2\Phi - (\nabla^2\Phi^*)\Phi\big]/2$, becomes

$$\langle -\nabla_i^2\rangle_{\rm JF} = \int \big[\Phi^* F^2\nabla_i^2\Phi - \tfrac{1}{4}F^2\nabla_i^2(\Phi^*\Phi) + \tfrac{1}{2}\Phi^*\big\{F\nabla_i^2 F - (\nabla_i F)^2\big\}\Phi\big] d^3r_1\ldots d^3r_N \ , \tag{3.1.19}$$

known as the Jackson-Feenberg (JF) form for the kinetic energy [14]

If the many-body integrations were carried out exactly, the PB, CW and JF forms of the kinetic energy would yield the same result. Hence, the discrepancies between the results obtained using different prescriptions provides a measure of the accuracy of the calculation of the expectation value.

3.2 Ground state energy

The energy per particle of a fluid of hard spheres of radius $a = 1$ fm and degeneracy $\nu = 2$ has been obtained by minimizing the expectation value of the hamiltonian in the correlated ground state, computed in the FHNC approximation. The final expressions corresponding to the CW and JF forms of the kinetic energy are

$$E_{\rm CW} = T_F + \frac{\rho}{2m}\int d^3r \left(\frac{\nabla f(r)}{f(r)}\right)^2 g(r) \ , \tag{3.2.1a}$$

$$\begin{aligned} E_{\rm JF} = T_F - \frac{\rho}{4m}\int d^3r \Bigg[&\big(\nabla^2 \ln f(r)\big)\, g(r) \\ &+ \frac{1}{2}(f^2(r)\, e^{N_{dd}} - 1)\Big(\frac{1}{\nu}\nabla^2\ell^2(k_F\, r) - 2N_{cc}\nabla^2\ell(k_F\, r)\Big)\Bigg]. \end{aligned} \tag{3.2.1b}$$

The correlation function has been chosen of the form

$$f(r) = \theta(d-r)\left\{\theta(r-a)\frac{d}{r}\,\frac{\sin[k_0(r-a)]}{\sin[k_0(d-a)]}\right\} + \theta(r-d) \ , \tag{3.2.2}$$

where $d > a$, $\theta(x)$ is the Heaviside theta-function and k_0 is determined in such a way as to have

$$\left(\frac{df}{dr}\right)_{r=d} = 0 \ . \tag{3.2.3}$$

For any value of the density the expectation value $E = \langle H \rangle / N$ has been minimized with respect to the correlation range d (see Eq.(3.2.2)). The shape of f corresponding to the minimum at $k_F = 0.5$ fm^{-1} is illustrated in Fig. 2.1 of Chapter 2.

The behavior of E as a function of d is displayed in Fig. 3.1, while Fig. 3.2 shows the k_F (i.e. density) dependence. For comparison we also report the results of a perturbative calculation up to order $(a\,k_F)^3$ (see Eq.(1.3.12)). It appears that the requirement that the FHNC energy be an upper bound to the ground state energy is always fulfilled.

In order to illustrate the dependence of the results on the hard core radius, in Fig. 3.3 we also show the results of the FHNC calculations of Ref. [15], carried out for a system of hard spheres of radius $a = 0.2$ fm and degeneracy $\nu = 4$. Comparison between Figs. 3.2 and 3.3 clearly demonstrates that the convergence of the perturbative expansion is driven by the product $x = a\,k_F$.

Finally in Table 3.4 we compare the values of the energy expectation values computed at two-body cluster level and within the FHNC approximation to the results of the perturbative low density expansions. To gauge the dependence of our results on the treatment of the kinetic energy, we also provide the ratio

$$\Delta = \frac{|E_{\rm JF} - E_{\rm CW}|}{E_{\rm JF}} \ . \tag{3.2.4}$$

It clearly appears that choosing the CW or JF form does not lead to significant differences.

3.3 CBF effective interaction

Within the CBF formalism, the effective interaction is defined through

$$\langle H \rangle = \frac{\langle \Phi_0 | FHF | \Phi_0 \rangle}{\langle \Phi_0 | FF | \Phi_0 \rangle} = T_F + \langle \Phi_0 | V_{\rm eff} | \Phi_0 \rangle \ , \tag{3.3.1}$$

T_F being the Fermi gas kinetic energy. The above equation shows that to obtain $V_{\rm eff}$ one has to carry out the calculation of the expectation value of the hamiltonian, e.g. within

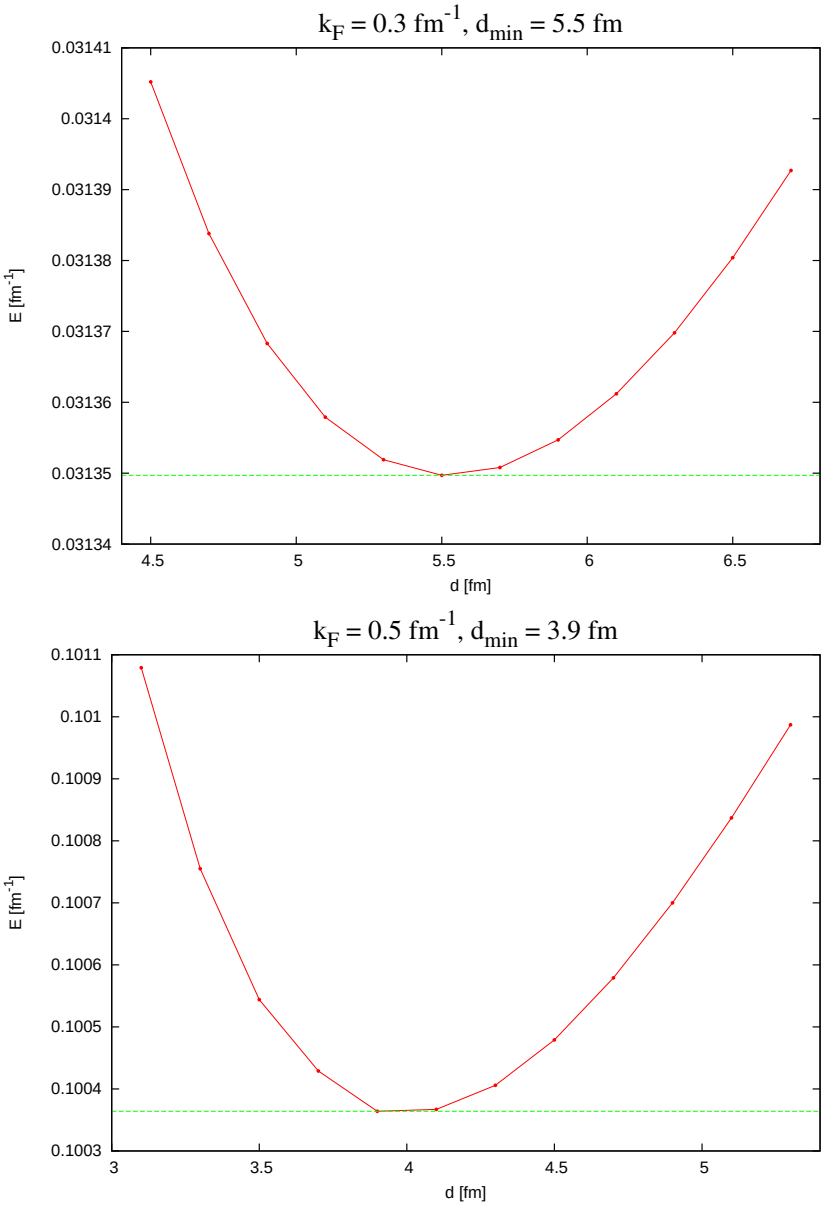

Figure 3.1: Minimization of the ground state energy of a system of fermion hard spheres of radius $a = 1$ fm and degeneracy $\nu = 2$, as a function of the correlation range d at Fermi momentum $k_F = 0.3$ fm^{-1} (upper panel) and 0.5 fm^{-1} (lower panel).

the FHNC approximation. An alternative strategy, originally proposed in Refs. [16, 17] is based on the use of low order approximations to $\langle H \rangle$. Within this approach, and

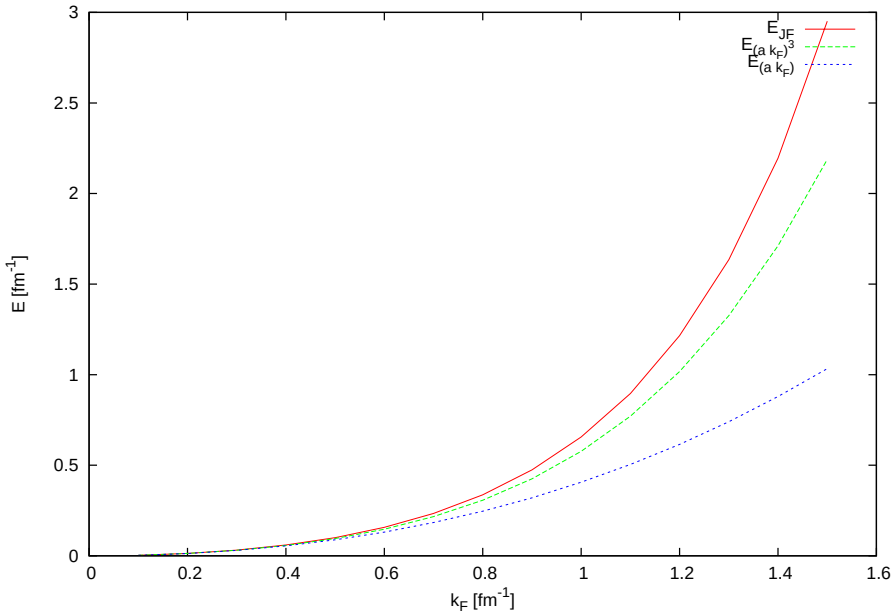

Figure 3.2: Fermi momentum dependence of the energy per particle of a system of fermion hard spheres of radius $a = 1$ fm and degeneracy $\nu = 2$. The lines correspond to the results obtained using FHNC and the perturbative low density expansion up to order $(a\,k_F)$ and $(a\,k_F)^3$.

keeping only the two-body cluster contribution, the effective potential takes the simple form (compare to Eq.(3.1.14))

$$V_{\rm eff} = \sum_{i<j} v_{\rm eff}(ij) = \sum_{i<j} \left[\frac{1}{m} (\boldsymbol{\nabla} f_{ij})^2 + v(ij) f_{ij}^2 \right] \ . \tag{3.3.2}$$

Note that in the case of hard spheres, as the correlation functions vanish at $r_{ij} < a$, the interaction energy arises from the kinetic term only.

All approaches based on effective interactions are designed to provide accurate estimates of the relevant physical quantities at low order in a given approximation scheme. Following this philosophy, we have determined the correlation functions appearing in Eq.(3.3.2) in such a way as to reproduce the FHNC energy at two-body level in the cluster expansion. This obviously implies that the range of the f_{ij}'s, i.e. the range of the

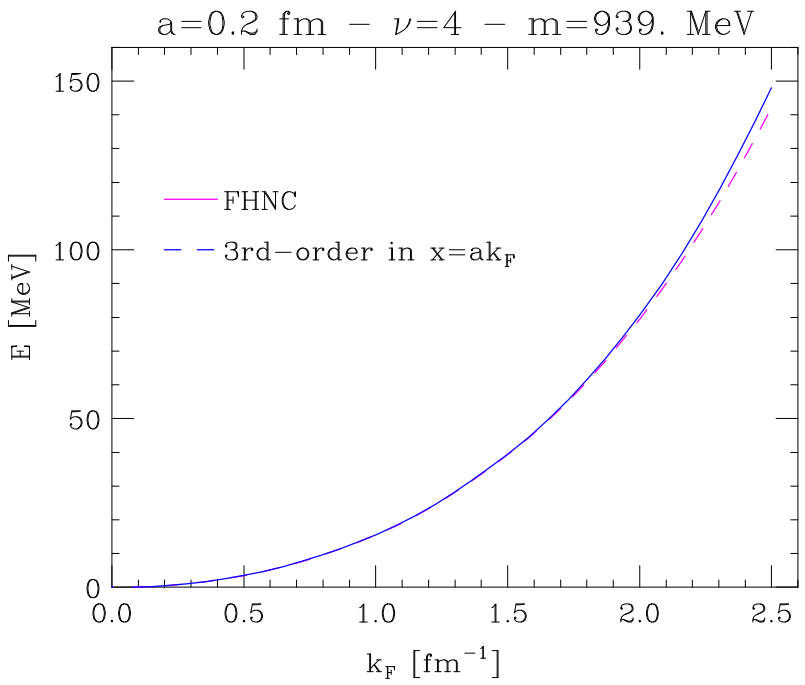

Figure 3.3: Same as in Fig. 3.2, but for a system of fermion hard spheres of radius $a = 0.2$ fm, mass $m = 939$ MeV and degeneracy $\nu = 4$.

effective potential, is *not* the same as the range of the correlation functions resulting from minimization of the FHNC energy. The results displayed in Fig. 3.5 show that in fact the range of the effective interaction turns out to be somewhat shorter at all densities.

The radial shape of the effective interaction at two different values of the Fermi momentum is shown in Fig. 3.6.

3.4 Transport properties

The quantitative description of transport properties of nuclear matter is relevant to the understanding of a variety of neutron star properties. Thermal conductivity is one of the driving factors of the cooling process, while electrical conductivity is relevant to the ohmic dissipation of magnetic fields in the star interior. In rotating stars, a crucial role is also played by viscosity, that determines the possible onset of the gravitational-wave

k_F	T_F	E_{2b}	E_{JF}	$E[(a\,k_F)]$	$E[(a\,k_F)^3]$	Δ
0.1	0.0030	3.12×10^{-3}	3.13×10^{-3}	3.11×10^{-3}	3.11×10^{-3}	1.15×10^{-4}
0.2	0.0120	1.30×10^{-2}	1.31×10^{-2}	1.28×10^{-2}	1.30×10^{-2}	3.82×10^{-4}
0.3	0.0270	3.08×10^{-2}	3.13×10^{-2}	2.99×10^{-2}	3.06×10^{-2}	8.43×10^{-4}
0.5	0.0750	9.60×10^{-2}	10.03×10^{-2}	8.83×10^{-2}	9.53×10^{-2}	2.29×10^{-3}
0.6	0.1080	1.46×10^{-1}	1.57×10^{-1}	1.31×10^{-1}	1.47×10^{-1}	3.01×10^{-3}
0.7	0.1470	2.13×10^{-1}	2.34×10^{-1}	1.83×10^{-1}	2.16×10^{-1}	4.09×10^{-3}
0.8	0.1920	2.98×10^{-1}	3.37×10^{-1}	2.46×10^{-1}	3.07×10^{-1}	5.07×10^{-3}
0.9	0.2430	4.04×10^{-1}	4.74×10^{-1}	3.20×10^{-1}	4.25×10^{-1}	6.18×10^{-3}
1.0	0.3000	0.531	0.656	0.406	0.577	6.74×10^{-3}
1.1	0.3630	0.693	0.896	0.504	0.771	8.01×10^{-3}
1.2	0.4320	0.886	1.215	0.615	1.02	8.65×10^{-3}
1.3	0.5070	1.12	1.64	0.740	1.33	9.95×10^{-3}
1.4	0.5880	1.42	2.19	0.879	1.71	1.19×10^{-2}
1.5	0.6750	1.77	2.95	1.03	2.19	1.28×10^{-2}

Figure 3.4: Energy per particle of a fluid of hard spheres of radius $a = 1$ fm and degeneracy $\nu = 2$, as a function of Fermi momentum. T_F is the kinetic energy of the non interacting Fermi gas, whereas E_{2b} and E_{JF} denote the two-body cluster approximation and the FHNC energy of Eq.(3.2.1b), respectively. The results of perturbation theory to order $(a\,k_F)$ and $(a\,k_F)^3$ are given by $E[(a\,k_F)]$ and $E[(a\,k_F)^3]$. The last column shows the function Δ defined in Eq.(3.2.4). Units are fm^{-1}.

driven instabilities first predicted by Chandrasekhar in the 1970s [18, 19].

The CBF effective interaction approach has been recently employed to evaluate the shear viscosity of both pure neutron matter [17] and nuclear matter in beta equilibrium [20]. To assess the validity of this scheme, we have carried out a similar calculation for the hard sphere fluid and compared the results to those obtained from the low density perturbative expansion.

The theoretical description of transport properties of normal Fermi liquids is based on Landau theory [21]. Working within this framework and including the leading term in the low-temperature expansion, Abrikosov and Khalatnikov [10] obtained the approximate

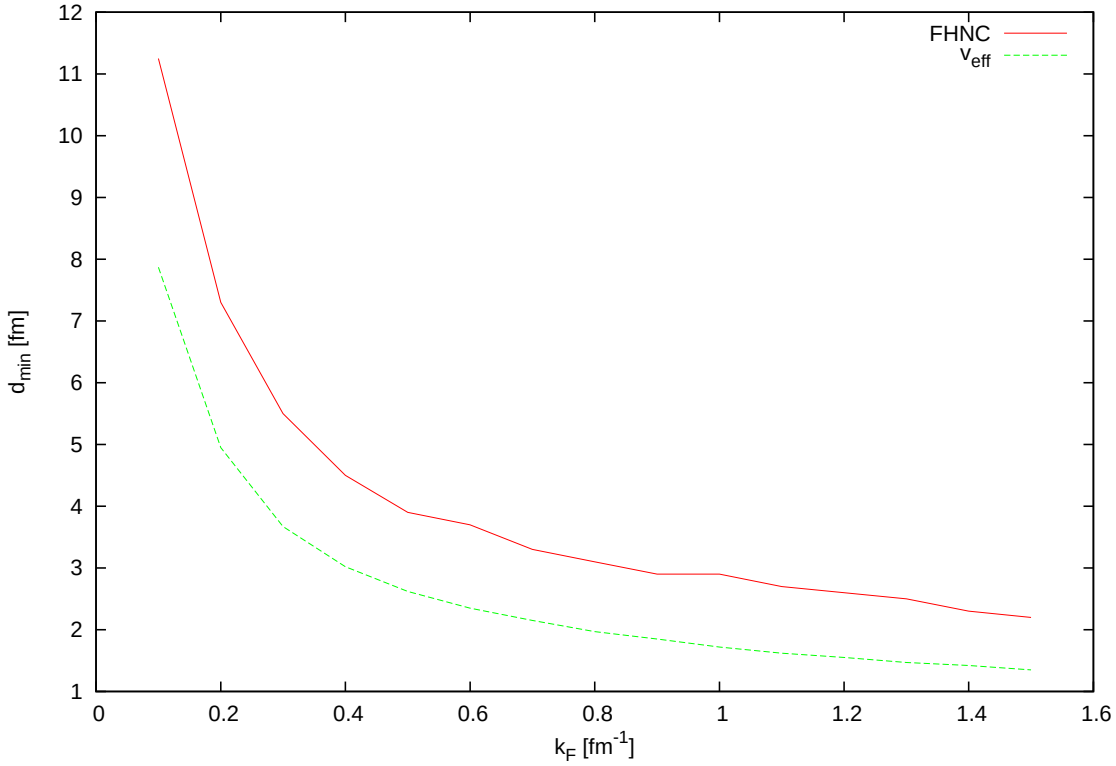

Figure 3.5: Comparison between the range of the correlation functions appearing in the definition of the effective potential, Eq.(3.3.2), (solid line) and that resulting from minimization of the FHNC energy (dashed line).

expression of the shear viscosity coefficient

$$\eta_{AK} = \frac{1}{5}\rho m^\star v_F^2 \tau \frac{2}{\pi^2(1-\lambda_\eta)} \ , \tag{3.4.1}$$

where $v_F = (\partial\epsilon/\partial k)_{|\mathbf{k}|=k_F}$, ϵ being the *quasiparticle* energy, is the Fermi velocity and $m^\star$ is the effective mass, defined through

$$\frac{1}{m^\star} = \frac{1}{k}\frac{d\epsilon}{dk} \ . \tag{3.4.2}$$

The quasi-particle lifetime τ can be written in terms of the angle-averaged scattering

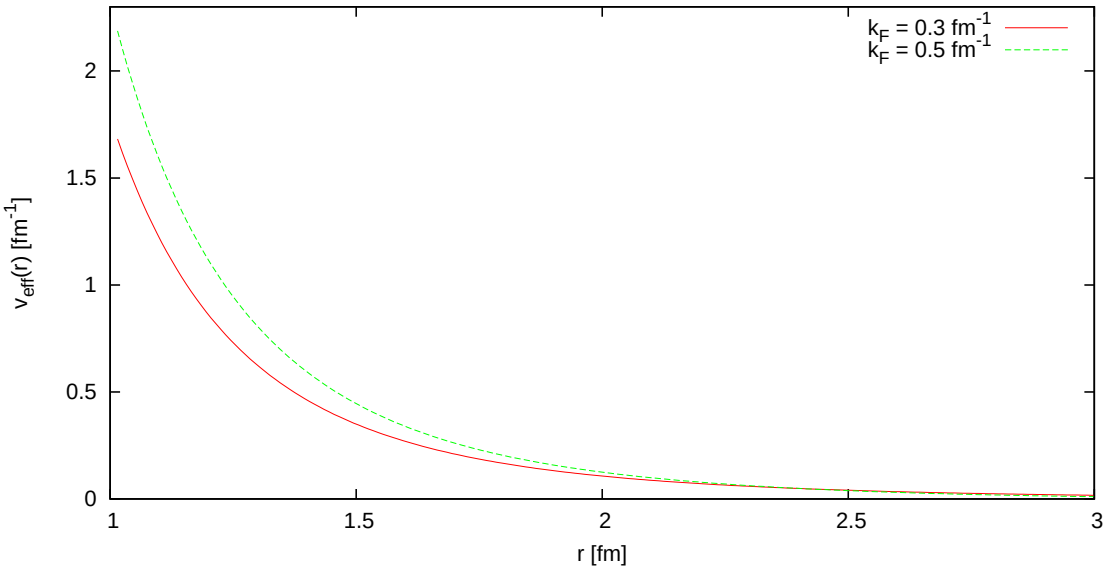

Figure 3.6: CBF effective interaction $v_{\rm eff}$, defined in Eq.(3.3.2), plotted as a function of r for Fermi momentum $k_F = 0.2$ and 0.3 fm^{-1}.

probability $\langle W \rangle$ according to

$$\tau T^2 = \frac{8\pi^4}{m^{*3}} \frac{1}{\langle W \rangle} \ , \tag{3.4.3}$$

where T is the temperature and

$$\langle W \rangle = \int \frac{d\Omega}{2\pi} \frac{W(\theta, \phi)}{\cos(\theta/2)} \ . \tag{3.4.4}$$

Note that the scattering process involves quasiparticles on the Fermi surface. As a consequence, for any given density ρ, W depends only on the angular variables θ and ϕ, the magnitude of all quasiparticle momenta being equal to the Fermi momentum. Finally,

the quantity λ_η appearing in Eq.(3.4.1) is defined as

$$\lambda_\eta = \frac{\langle W[1 - 3\sin^4(\theta/2)\sin^2\phi]\rangle}{\langle W\rangle} \ . \tag{3.4.5}$$

The exact solution of the equation derived in Ref. [10], obtained by Brooker and Sykes [22], reads

$$\begin{aligned} \eta &= \eta_{AK}\ \frac{1-\lambda_\eta}{4} \\ &\times \sum_{k=0}^{\infty} \frac{4k+3}{(k+1)(2k+1)[(k+1)(2k+1)-\lambda_\eta]} \ , \end{aligned} \tag{3.4.6}$$

the size of the correction with respect to the result of Eq.(3.4.1) being

$$0.750 \ < \ (\eta/\eta_{AK}) \ < \ 0.925 \ . \tag{3.4.7}$$

Equations (3.4.1)-(3.4.6) show that the key element in the determination of the viscosity is the in-medium scattering cross section. The relation between scattering in vacuum and in matter has been often analyzed under the assumption that the medium mainly affects the flux of incoming particles and the phase space available to the final state particles, while leaving the transition probability unchanged. Within this picture $W(\theta,\phi)$ can be extracted from the scattering cross section in free space, $(d\sigma/d\Omega)_{\rm vac}$, according to

$$W(\theta,\phi) = \frac{16\pi^2}{m^{\star 2}} \left(\frac{d\sigma}{d\Omega}\right)_{\rm vac} \tag{3.4.8}$$

where $m^\star$ is the nucleon effective mass and θ and ϕ are related to the kinematical variables in the center of mass frame through [23]

$$E_{cm} = \frac{k_F^2}{2m}(1-\cos\theta) \quad , \quad \theta_{cm} = \phi \ . \tag{3.4.9}$$

The CBF effective interaction defined in Eq.(3.3.2) can be employed to obtain the scattering probability of Eq.(3.4.8) from Fermi's golden rule

$$W(\theta,\phi) = \ |\hat{v}_{\rm eff}(\mathbf{q})|^2 \ , \tag{3.4.10}$$

$\hat{v}_{\rm eff}(\mathbf{q})$ being the Fourier transform of the effective potential at momentum transfer $\mathbf{q}$, whose magnitude is given by

$$|\mathbf{q}| = \sqrt{2m\, E_{\rm cm}(1-\cos\phi)}\ . \tag{3.4.11}$$

Figure 3.7 shows the ϕ-dependence of $W(\theta,\phi)$ for $\theta = 0,\ \pi/2$ and π, at Fermi momentum $k_F = 0.2$ and 0.5 fm^{-1}. We have verified that, in the low density limit, the total cross section obtained from the scattering probability illustrated in Fig. 3.7 approaches its value in vacuum, discussed in Appendix A.

The temperature independent quantity ηT^2, computed using the CBF effective interactions and the effective masses evaluated following the procedure discussed in Ref. [17], is displayed in Fig. 3.8 as a function of density. The results of the approach discussed in this thesis are compared to those obtained from the low density perturbative expansion, including terms up to order $(a\,k_F)^2$ [24].

$$\eta = 4.35\times 10^{-3}\left(\frac{k_F}{a^2}\right)\left(\frac{T_F}{T}\right)^2\left[1+0.208(a\,k_F)+O(a\,k_F)^2\right]\ . \tag{3.4.12}$$

Comparison of the results shown in Fig. 3.8 and those of Refs. [17, 20] suggests that the low order perturbative results does not include the full effect of screening arising from correlations. However, a systematic analysis of the differences between the elements underlying the perturbative and CBF approaches is called for.

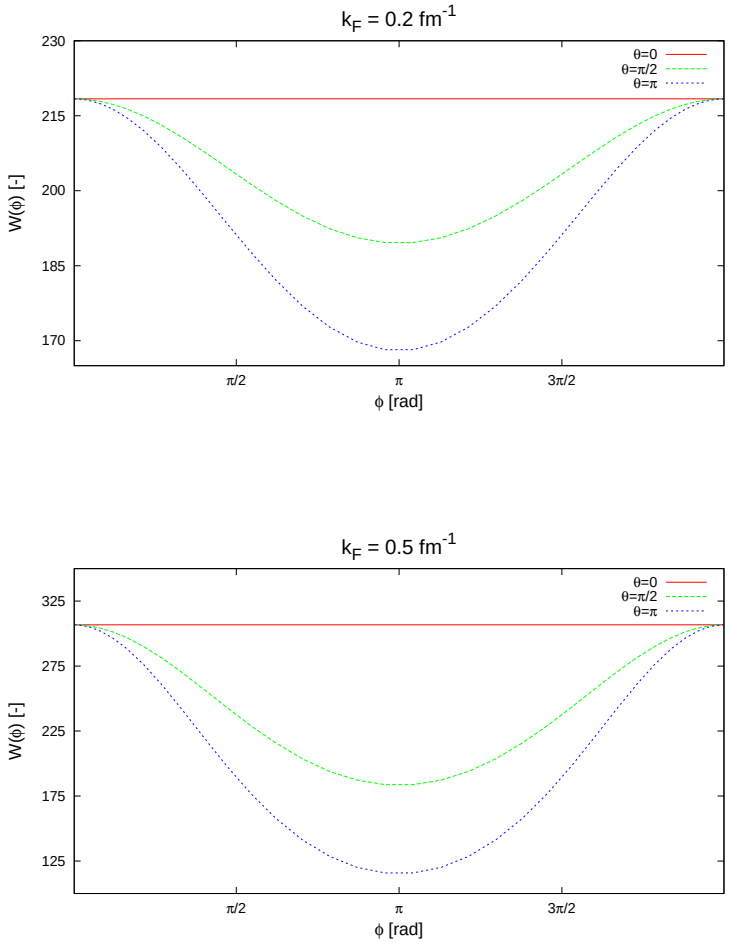

Figure 3.7: Scattering probability $W(\theta, \phi)$, plotted as a function of $\phi = \theta_{\rm cm}$ for three fixed values of $\theta = 0,\ \pi/2$ and π. The upper and lower panel correspond to Fermi momentum $k_F = 0.3$ and 0.5 fm^{-1}, respectively.

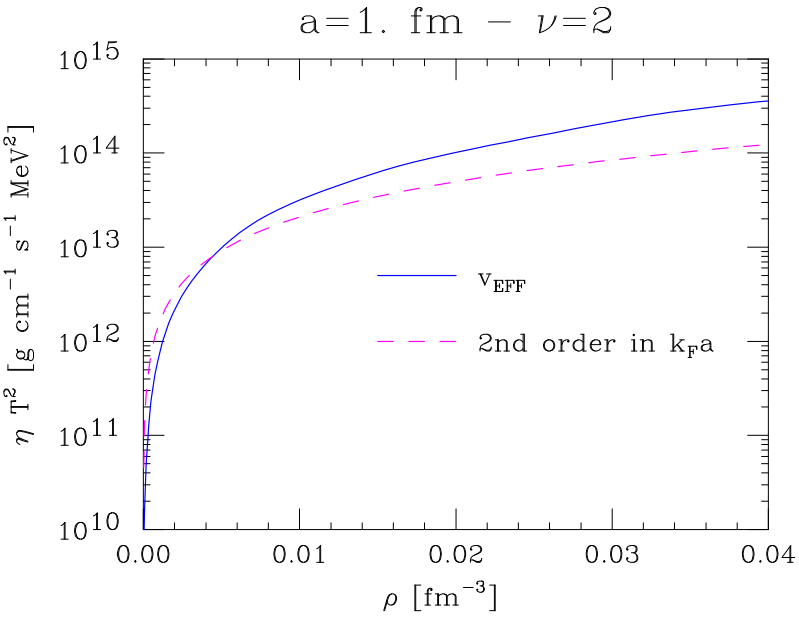

Figure 3.8: Density dependence of the quantity ηT^2 obtained using the CBF effective interaction (solid line) and the perturbative expansion in $x = a\,k_F$ [24].

Conclusions

In this thesis we have discussed a calculation of equilibrium and non equilibrium properties of a fluid of fermion hard spheres, carried out within a fully consistent framework.

The approach we employed to handle the strong repulsive core of the interaction potential, the treatment of which in standard perturbation theory involves severe difficulties, is based on CBF theory and the formalism of cluster expansion.

The calculation of the energy per particle as a function of density, which amounts to the determination of the equation of state at zero temperature, has been carried out solving the set of FHNC integral equations, allowing one to sum the relevant contributions at all orders of the cluster expansion.

The results of these calculations show that the FHNC energies are in good agreement with those obtained from perturbative calculations in the region in which the low density expansion is expected to be applicable. In addition, they always satisfy the requirement of providing an upper bound to the true ground state energy.

As recently shown [17, 20], the CBF formalism can be also exploited to obtain an effective interaction, suitable for calculating the collision integral appearing in the Landau-Boltzmann equation. The availability of this effective interaction allows one to carry out a *consistent* analysis of equilibrium and non equilibrium properties of interacting many-body systems based on the same dynamical model.

We have derived the CBF effective interaction for the fermion hard sphere systems and computed the shear viscosity coefficient, which has been also analyzed using the

perturbative low density expansion [24].

Comparison between CBF and perturbative results suggest that, while a careful analysis of the differences between the elements underlying the two approaches is in order, the perturbative result does not fully include the effects of screening of the bare interaction arising from correlations, which leads to a significant enhancement of the shear viscosity.

The investigation of the sources of discrepancies between perturbative and CBF prediction of the transport coefficient represents the natural extension of this thesis work. It will involve the calculation of thermal conductivity, which is known to be only sensitive to the total in-medium scattering cross section [25], as well as a careful comparison of the density dependence of the effective masses.

Appendix A

Partial wave expansion of the scattering amplitude

Choosing the z-axis along the wake-vector $\mathbf{k}$ the direction of $\mathbf{k}'$ is specified by the polar and azimuthal angles θ and φ, respectively.
Obviously, if we deal with a spherically symmetric potential, the scattering amplitude is a function of θ only, i.e.

$$f(\theta, \varphi) = f(\theta) \ ,$$

and neither the incident nor the total wave-function depend on the azimuthal angle φ:

$$\phi(\mathbf{r}) = \frac{e^{ikr\cos\theta}}{(2\pi)^{3/2}}, \quad \psi(\mathbf{r}) = \phi(\mathbf{r}) + \frac{f(\theta)}{(2\pi)^{3/2}}\frac{e^{ikr}}{r}. \tag{A.0.1}$$

Outside the range of $V(r)$ both $\psi(\mathbf{r})$ and $\phi(\mathbf{r})$ satisfy

$$(\nabla^2 + k^2)\psi = 0. \tag{A.0.2}$$

The most general solution of the above equation can be obtained carrying out the partial-wave decomposition, which amounts to expanding in Legendre Polynomials according to

[1]

$$\psi(r,\theta) = \sum_l R_\ell(r) P_\ell(\cos\theta) \ . \tag{A.0.3}$$

Substitution of the above expansion in Eq.(A.0.2) yields a set of second order differential equations for the functions $R_\ell(r)$, whose independent solutions are the spherical Bessel functions $j_\ell(kr)$ and the Neumann functions $\eta_\ell(kr)$:

$$j_\ell(y) = y^\ell \Big(-\frac{1}{y}\frac{d}{dy}\Big)^\ell \frac{\sin y}{y}, \tag{A.0.4a}$$

$$\eta_\ell(y) = y^\ell \Big(-\frac{1}{y}\frac{d}{dy}\Big)^\ell \frac{\cos y}{y}. \tag{A.0.4b}$$

It should be noted that while the Bessel functions $j_\ell(y)$ are well-behaved everywhere, the Neumann functions are singular in the limit $y \to 0$; the asymptotic behaviour in the limit $y \to \infty$ is

$$j_\ell(y) \to \frac{\sin(y - \ell\pi/2)}{y}, \quad \eta_\ell(y) \to -\frac{\cos(y - \ell\pi/2)}{y}. \tag{A.0.5}$$

The most general expression of the total wave-function *outside the scattering region* is

$$\psi(\mathbf{r}) = \frac{1}{(2\pi)^{\frac{3}{2}}} \sum_\ell \Big[A_\ell \, j_\ell(kr) + B_\ell \, \eta_\ell(kr) \Big] P_\ell(\cos\theta), \tag{A.0.6}$$

which in the large-r limit, using Eq.(A.0.5), reduces to

$$\psi(\mathbf{r}) \simeq \frac{1}{(2\pi)^{\frac{3}{2}}} \sum_\ell C_\ell \frac{\sin(kr - \ell\pi/2 + \delta_\ell)}{kr} P_\ell(\cos\theta), \tag{A.0.7}$$

where we have combined the sine and cosine functions to obtain a sine function shifted by a phase δ_ℓ. In this way we have decomposed the wave into a series of spherical-waves called *partial waves*.

Developing the sine function of Eq.(A.0.7) into exponentials we see that $\psi(\mathbf{r})$ contains

[1] The Legendre polynomials are related to the spherical harmonics via

$$P_l(\cos\theta) = \sqrt{\frac{4\pi}{2l+1}} Y_l^0(\theta,\varphi)$$

both incoming and outgoing spherical waves whereas we expect only the outgoing ones. Therefore, the incoming waves must originate from the large-r asymptotic expansion of the incident wave-function $\phi(\mathbf{r})$ and they cancel when we carry out the subtraction

$$(2\pi)^{3/2}\big[\psi(\mathbf{r}) - \phi(\mathbf{r})\big] = \frac{e^{ikr}}{r} f(\theta). \tag{A.0.8}$$

This condition implies that the coefficients of the expansions of $\psi(\mathbf{r})$ and $\phi(\mathbf{r})$ must be equal (see appendix B for details), it follows that

$$C_\ell = (2\ell+1)e^{i(\delta_\ell + \ell\pi/2)} \ . \tag{A.0.9}$$

Finally, from Eq.(A.0.7)-(A.0.9) we obtain

$$f(\theta) = \sum_{\ell=0}^{\infty} (2\ell+1)\frac{e^{i\delta_\ell}}{k} \sin\delta_\ell \, P_\ell(\cos\theta), \tag{A.0.10}$$

which is the decomposition of the scattering amplitude $f(\theta)$ in partial waves with phase-shifts δ_ℓ.

A.1 Optical theorem

Let us now consider the total cross-section

$$\sigma = \int \frac{d\sigma}{d\Omega} d\Omega = \int |f(\theta)|^2 d\Omega \ . \tag{A.1.1}$$

We can perform the integration using Eq.(A.0.10) and the orthonormality relations fulfilled by Legendre polynomials, with the result

$$\sigma = \frac{4\pi}{k^2} \sum_\ell (2\ell+1)\sin^2\delta_\ell. \tag{A.1.2}$$

Comparison between Eq.(A.0.10) and Eq.(A.1.2) yields the result [2]

$$\sigma = \frac{4\pi}{k}\,\Im\{f(0)\}, \tag{A.1.3}$$

[2]Note that $P_\ell(1) = 1$

known as *optical theorem*. It states the fact that scattering in the *forward* direction ($\theta = 0$) is always non-zero. Thus, there will always be a bright spot in the shadow in the forward direction, produced by the destructive interference between the incident plane-wave $e^{ikr\cos\theta}$ and the scattered wave $f(\theta)e^{ikr}/r$.

Writing

$$\sigma = \sum_{\ell=0}^{\infty} \sigma_\ell,$$

we can introduce the ℓ-th partial cross-section

$$\sigma_\ell = \frac{4\pi}{k^2}(2\ell+1)\sin^2\delta_\ell, \tag{A.1.4}$$

i.e. the contribution to σ from the ℓ-th partial wave.

From the above results it follows that the value of the phase-shift completely determines the scattering process. The cross-section vanishes for $\delta_\ell = 0, \pi$ and reaches its maximum value for $\delta_\ell = \pi/2$.

To see how the phase-shifts can be evaluated let us consider the specific case of a spherically symmetric potential $V(r)$ that vanishes for $r > a$, where a is the potential range.

The most general form of the wave-function $\psi(\mathbf{r})$ in the region $r > a$, i.e. the solution of the free-space Schrödinger equation Eq.(A.0.2), is

$$\psi(\mathbf{r}) = \frac{1}{(2\pi)^{\frac{3}{2}}}\sum_\ell i^\ell(2\ell+1)A_\ell(r)\,P_\ell(\cos\theta), \tag{A.1.5}$$

where

$$A_\ell(r) = e^{i\delta_\ell}[\cos\delta_\ell\, j_\ell(kr) - \sin\delta_\ell\,\eta_\ell(kr)]. \tag{A.1.6}$$

The logarithmic derivative of $A_\ell(r)$ for $r = a$ is

$$\gamma_\ell \equiv \frac{A'_\ell(r)}{A_\ell(r)}\Big|_{r=a} = ka\,\frac{\cos\delta_\ell\, j'_\ell(ka) - \sin\delta_\ell\,\eta'_\ell(ka)}{\cos\delta_\ell\, j_\ell(ka) - \sin\delta_\ell\,\eta_\ell(ka)}, \tag{A.1.7}$$

where $g'(x) = dg(x)/dx$. We can invert this relation to obtain

$$\tan\delta_\ell = \Big[\frac{ka\, j'_\ell(ka) - \gamma_\ell\, j_\ell(ka)}{ka\,\eta'_\ell(ka) - \gamma_\ell\,\eta_\ell(ka)}\Big]. \tag{A.1.8}$$

A.2 Hard sphere scattering

Finally, let us consider scattering by a hard sphere.

In this case, the potential is infinite for $r \leq a$ and 0 everywhere else.

The wave-function $\psi(\mathbf{r})$ is zero for $r \leq a$, which implies $A_\ell(r) = 0 \quad \forall\, \ell$, yielding

$$\gamma_\ell = \infty \quad \forall\, \ell \ .$$

Hence, from Eq.(A.1.8) it follows that

$$\tan \delta_\ell = \frac{j_\ell(ka)}{\eta_\ell(ka)}. \tag{A.2.1}$$

Consider the $\ell = 0$ partial wave (s-wave). From Eqs.(A.0.4a)-(A.0.4b) we obtain

$$\tan \delta_0 = \frac{\sin(ka)/ka}{-\cos(ka)/ka} = -\tan(ka), \tag{A.2.2}$$

i.e.

$$\delta_0 = -ka. \tag{A.2.3}$$

The s-wave radial wave-function, given by Eq.(A.1.6), is

$$A_0(r) = e^{-ika}\frac{\sin k(r-a)}{kr}, \tag{A.2.4}$$

while the corresponding radial wave-function for the incident wave is

$$\tilde{A}_0(r) = \frac{\sin kr}{kr} \ . \tag{A.2.5}$$

The radial s-wave wave functions for the scattered and the incident waves are similar, but shifted by a phase ka.

We can now discuss the low energy limit ($ka \ll 1$) of Eq.(A.2.1)[3]

$$\tan \delta_\ell \simeq -\frac{(ka)^{2\ell+1}}{(2\ell+1)[(2\ell-1)!!]^2}, \tag{A.2.6}$$

[3]Recall that

$$j_\ell(y) \xrightarrow[y\to 0]{} \frac{y^\ell}{(2\ell+1)!!},\ \eta_\ell(y) \xrightarrow[y\to 0]{} -\frac{(2\ell-1)!!}{y^{\ell+1}},\ (2\ell+1)!! = 1\cdot 3\cdots(2\ell+1)$$

showing that δ_ℓ falls off rapidly as ℓ increases, and vanishes as $k \to 0$.

However, the s-wave remains finite, because of the $1/k^2$ factor of Eq.(A.1.2). Hence, at low energy only s-wave scattering (which is spherically symmetric) contributes to the cross section.

For $ka \ll 1$ we can write

$$\frac{d\sigma}{d\Omega} = \frac{\sin^2 ka}{k^2} \simeq a^2, \tag{A.2.7}$$

and the corresponding total cross-section

$$\sigma = 4\pi a^2, \tag{A.2.8}$$

turns out to be four times the *geometric* cross-section πa^2 (i.e. the classical cross-section for the hard sphere problem). This is not surprising, because the low-energy limit corresponds to to long wave-lengths ($ka = 2\pi/\lambda$), and we do not expect to find the classical result.

If we consider instead the high energy limit ($ka \gg 1$), using the asymptotic forms of j_ℓ and η_ℓ given by Eq.(A.0.5), it easy to see that all partial wave up to $\ell_{\max} = ka$ contribute significantly to the cross-section:

$$\sigma = \frac{4\pi}{k^2} \sum_{\ell=0}^{\ell_{\max}} (2\ell + 1) \sin^2 \delta_\ell \ . \tag{A.2.9}$$

In this case, we can replace $\sin^2 \delta_\ell$ with its average value, $1/2$, with the result

$$\sigma \simeq \frac{2\pi}{k^2} \sum_{\ell=0}^{ka} (2\ell + 1) = 2\pi a^2, \tag{A.2.10}$$

which is twice the classical result.

This time the outcome is somewhat surprising, since we might expect the classical result. High energies correspond indeed to short wave-lengths, so that wave-packets are small compared with the size of the scattering region. These wave-packets will follow approximately classical trajectories.

The reason of this apparent anomaly is that the scattering is counted twice in the classical limit. Once in the true scattering (which is spherically symmetric) and once in the shadow of the scattering sphere in the forward direction produced by destructive interference between incident plane wave and scattered one. The optical theorem assures that the interference is not completely destructive so that the shadow has a bright spot, to which is associated an effective cross-section πa^2. Thus we totally get $2\pi a^2$.

Appendix B

Calculation of the partial wave coefficients C_ℓ

Let us start expanding the incident wave-function around the scattering zone in the Legendre-functions' basis:

$$e^{ikr\cos\theta} = \sum_\ell a_\ell \, j_\ell(kr) \, P_\ell(\cos\theta) \ . \tag{B.0.1}$$

Note that Neumann functions are absent because they are not well-behaved for $r \to 0$. Using the orthonormality of the Legendre functions

$$\int_{-1}^{1} P_n(\mu) P_m(\mu) d\mu = \frac{\delta_{nm}}{n + 1/2},$$

we can invert Eq.(B.0.1) to obtain

$$a_\ell \, j_\ell(kr) = (l + \ell/2) \int_{-1}^{1} e^{ikr\mu} \, P_\ell(\mu) d\mu. \tag{B.0.2}$$

A useful property of Bessel functions is [26]:

$$j_\ell(y) = \frac{(-1)^\ell}{2} \int_{-1}^{1} e^{iy\mu} \, P_\ell(\mu) d\mu,$$

which implies

$$a_\ell = i^\ell (2\ell + 1) \ .$$

Hence

$$e^{ikr\cos\theta} = \sum_\ell i^\ell (2\ell+1)\, j_\ell(kr)\, P_\ell(\cos\theta). \tag{B.0.3}$$

In the large-r limit this expression can be developed using the asymptotic form of $j_\ell(kr)$:

$$\phi(\mathbf{r}) = \frac{1}{(2\pi)^{\frac{3}{2}}} \sum_\ell i^l (2\ell+1)\, \frac{e^{i(kr-\ell\pi/2)} - e^{-i(kr-\ell\pi/2)}}{2i\,kr}\, P_\ell(\cos\theta). \tag{B.0.4}$$

If we now compare this expression with the asymptotic form of the total wave-function

$$\psi(\mathbf{r}) = \frac{1}{(2\pi)^{\frac{3}{2}}} \sum_\ell C_\ell\, \frac{e^{i(kr-\ell\pi/2+\delta_\ell)} - e^{-i(kr-\ell\pi/2+\delta_\ell)}}{2i\,kr}\, P_\ell(\cos\theta), \tag{B.0.5}$$

and use

$$(2\pi)^{3/2}\big[\psi(\mathbf{r}) - \phi(\mathbf{r})\big] = \frac{e^{ikr}}{r} f(\theta),$$

we find the definition of C_ℓ:

$$C_\ell = (2\ell+1)e^{i(\delta_\ell+\ell\pi/2)},$$

QED.

Bibliography

[1] J.P. Hansen and I.R. McDonald, *Theory of Simple Liquids*, (Academic Press, London, 1986).

[2] A.L. Fetter and J.D. Walecka, *Quantum theory of Many-Particles systems* (McGraw-Hill, New York, 1971).

[3] L.I. Schiff, *Quantum mechanics*, McGraw-Hill, New York, 1949).

[4] E. Feenberg, *Theory of Quantum Fluids* (Academic Press, New York, 1969).

[5] S.A. Rice and P. Gray, *The statistical mechanics of simple liquids* , (Interscience, New York, 1965).

[6] R. Jastrow, Phys. Rev. **98** (1955) 1479.

[7] S. Rosati, (1981) *FHNC variational theory for strongly interacting systems*, Proc. Int. School E. Fermi, Course LXXIX.

[8] S. Fantoni and S. Rosati, Nuovo Cimento A, **20** (1974) 179.

[9] S. Fantoni and S. Rosati, Nuovo Cimento A, **25** (1975) 593.

[10] A.A. Abrikosov and I.M. Khalatnikov, Soviet Phys. JETP **5** (1957) 887; Rep. Prog. Phys. **22** (1959) 329.

[11] J.W. Clark, Prog. Part. Nucl. Phys. **2** (1979) 89.

[12] V.R. Pandharipande and H.A. Bethe, Phys. Rev. C **7** (1973) 1312.

[13] J.W. Clark and P. Westhaus. Phys. Rev C **141** (1966) 833.

[14] H.W. Jackson and E. Feenberg, Ann. Phys. **15** (1961) 266.

[15] J.G. Zabolitzky, Phys. Lett. **64B** (1976) 233.

[16] S. Cowell and V.R. Pandharipande, Phys. Rev. C, **73** (2006) 025801.

[17] O. Benhar and M. Valli, Phys. Rev. Lett. **99** (2007) 232501.

[18] S. Chandrasekhar, Phys. Rev. Lett. **24** (1970) 611.

[19] S. Chandrasekhar, Astrophys. J. **161** (1970) 561.

[20] O. Benhar and A. Carbone, Phys. Rev. C, in press.

[21] G. Baym and C. Pethick, *Landau Fermi-Liquid Theory* (John Wiley & Sons, New York, 1991).

[22] G.A. Brooker and J. Sykes, Phys. Rev. Lett. **21** (1968) 279.

[23] E. Flowers and N. Itoh, Astrophys. J. **230** (1979) 847.

[24] J.C. Rainwater and F. Mohling, J. Low Temp. Phys. **23** (1976) 519.

[25] O. Benhar, A. Polls, M. Valli and I. Vidaña, Phys. Rev. C **81** (2010) 024305.

[26] M.Abramowitz and I.Stegun (Editors), *Handbook of Mathematical Functions* (Dover, New York, 1965).